Nonaqueous microemulsions stabilised by soybean phosphatidylcholine: effect of non-polar solvent molecular structure

Simona H. Kolarova[a], Thaslima Sultana[a], Georgina A. I. Critchley[a], Luke J. Hibbert[a],

Ann E. Terry[b,1], Simon P. King[c], L. Gino Martini[a,2], M. Jayne Lawrence[a,3]*, Cécile A. Dreiss[a]*

[a]Institute of Pharmaceutical Science, School of Cancer Studies and Pharmaceutical Science, King's College London, London, SE1 9NH, United Kingdom

[b]ISIS Neutron and Muon Source, Science and Technology Facilities Council, Rutherford Appleton Laboratory, Didcot, Oxfordshire, OX11 0QX, United Kingdom

[c]GSK Consumer Healthcare R&D, Weybridge, KT13 0DE, United Kingdom

*Corresponding Authors

E-mail: cecile.dreiss@kcl.ac.uk (Cécile A. Dreiss)
E-mail: jayne.lawrence@manchester.ac.uk (M. Jayne Lawrence)

[1] Present address: MAX IV Laboratory, Lund University, P.O. Box 118, Lund, 221 00, Sweden
[2] Present address: Royal Pharmaceutical Society, London, E1W 1AW, United Kingdom
[3] Present address: Division of Pharmacy & Optometry, University of Manchester, Manchester, M13 9PL, United Kingdom

Abstract. The preparation and characterisation of nonaqueous microemulsions employing pharmaceutically acceptable components, namely, soybean phosphatidylcholine (SPC) as surfactant, propylene glycol (PG) as polar solvent and fatty acid esters (FAE) as oil, are presented. The effect of FAE molecular structure (*i.e.*, molecular volume (MV), branching and saturation) on the systems' self-assembly was assessed using phase behaviour, dynamic light scattering (DLS), small-angle neutron scattering (SANS) and Langmuir trough (LT) monolayer compression. The results suggest that the systems' properties are primarily influenced by variations in FAE MV, while FAE branching and saturation have a limited effect.

All PG/SPC/FAE phase diagrams comprise large areas of microemulsion existence. Variations in phase behaviour with FAE MV were attributed to changes in both the FAE partition into the SPC interface and the monolayer bending elastic modulus, K. SANS data suggest a triaxial ellipsoidal morphology for FAE-in-PG microemulsions. The droplet's dimensions are strongly influenced by both the MV and concentration of FAE and these correlations were also attributed to changes in FAE interfacial partition and monolayer K. The proposed relationships between FAE MV, concentration and interfacial partition are upheld by DLS results, while the LT monolayer compression studies support the association between FAE MV and K.

Keywords. microemulsion, nonaqueous, soybean phosphatidylcholine, propylene glycol, fatty acid ester, phase behaviour, dynamic light scattering, small-angle neutron scattering, Langmuir trough.

Abbreviations. $\Delta\rho$, difference in neutron scattering length densities; π, surface pressure; π_{coll}, collapse surface pressure; K, bending elastic constant; A_c, surface area per complex; $A_{c,lim}$, limiting surface area per complex; C_s^{-1}, compressibility modulus; d_6-PG, 1,2-propane-d_6-diol; d_{15}-$R_2R'_{8:0}$, ethyl d_{15}-caprylate; d_{31}-PO, 1-palmitoyl-d_{31}-2-oleoyl; d_{31}-POPC, 1-palmitoyl-d_{31}-2-oleoyl-*sn*-glycero-3-phosphocholine; FA, fatty acid; FAlc, fatty alcohol; FAE, fatty acid ester; LT, Langmuir trough; NPS, non-polar solvent; PC, phosphatidyl choline; PG, propylene glycol; PO, 1-palmitoyl-2-oleoyl; POPC, 1-palmitoyl-2-oleoyl-sn-glycero-3-phosphocholine; PS, polar solvent; R, alcohol group; R′, fatty acid group; SLD, scattering length density; SPC, soybean phosphatidyl choline.

Introduction

More than 70 years ago, *Hoar* and *Schulman* first described the formation of transparent, isotropic and thermodynamically stable dispersions of oil and water in the presence of relatively large amounts of surfactant and cosurfactant and attributed it to the existence of uniform 'micelle-like' droplets of water or oil termed 'microemulsions'.[1,2] Since then, these self-aggregates have received increasing attention due to their desirable formulation properties, such as long-term stability,[3] nanometre size,[3] clarity[4,5] and modifiable viscosity,[4] and their ability to solubilize hydrophilic and/or lipophilic materials,[5] which make them excellent vehicles in a number of areas. For instance, microemulsions have been employed in the fields of oil extraction,[6] nanoparticle synthesis,[7] and enzyme catalysis.[8] Nonetheless, few commercial food- and drug-grade microemulsions have been developed over the years,[9] mainly due to the need for high surfactant concentrations and/or non-biocompatible cosurfactants[5,10-14] to promote microemulsification, both of which could lead to toxicological issues.[5,15] To address this problem, the aim of this work is to increase the understanding of the formation and properties of pharmaceutically acceptable nonaqueous microemulsions.

For this purpose, the generally regarded as safe (GRAS)[16] lipid soybean phosphatidylcholine (SPC), which is commercially employed in a variety of baked goods, confections and beverages,[17] as well as mixed micellar drug delivery formulations (such as Valium® MM and Konakion® MM),[18] was selected as the surfactant. SPC is a zwitterionic, twin-tailed phospholipid,[19] which has a critical packing parameter ($CPP = \frac{v}{a_o l}$, where v is tail volume, l is tail length and a_o is head group area)[20] of ~ 1[21] and comparable hydrophilicity and lipophilicity.[22] Owing to its well-balanced packing and hydrophilic-lipophilic properties,[23,24] the preferred interfacial curvature, C_0, of SPC interfaces in water and/or oil is close to zero.[25] Additionally, phosphatidylcholine (PC) lipids typically form aggregates of relatively high bending elastic constant, K ($K \sim 50\ k_B T$, where

k_B is the Boltzmann constant and T is temperature),[26] which suggest a macroscopic persistence length, ξ_K, for saturated SPC interfaces ($\xi_K = a \exp\left(\frac{2\pi K}{k_B T}\right)$, where a is the molecular length of the surfactant).[27] Together, the near-zero C_0 and relatively high ξ_K values favour the formation of planar SPC-stabilised structures of long-range order,[27] *e.g.*, lamellar, nematic, hexagonal and cubic phases, in water (and oil).[19,21,28]

To obtain SPC-stabilised microemulsions, the interfacial layer's K must be sufficiently lowered ($K < 1\ k_B T$)[24,29] to allow the formation of fluid interfaces ($\xi_K \sim 10\ a$),[27] while C_0 can be tuned *via* changes in the system's composition and environment to alter the preferred type of microemulsion (C_0 is positive, negative or close to zero for oil-in-water, water-in-oil or bicontinuous microemulsions, respectively).[24] This is typically achieved by the addition of a second amphiphile, which can affect both K and C_0 of a saturated surfactant interface by incorporating into it.[27] In systems employing SPC as the surfactant, such additional amphiphiles are most commonly either surfactants (such as rhamnolipids,[30] sophorolipids[30] and polysorbates[11]), cosurfactants (such as alcohols,[10,12-14] alkanoic acids,[13] alkanediols,[13] diethylene glycol alkyl ethers[13] and amines[13]) or a combination of the above.[31] Alternatively, to avoid the use of large amounts of surfactants and/or non-biocompatible cosurfactants, the substitution of water with a nonaqueous polar solvent (PS) has been explored as a method of promoting microemulsification in SPC-stabilised systems.[32-34] Depending on the PS employed, such nonaqueous systems can produce microemulsions over a significantly extended range of compositions[33] when compared to equivalent aqueous systems containing an additional surfactant[11] or cosurfactant,[10,12-14] thereby making them better-suited to a variety of commercial applications from a biocompatibility and tailorability perspective.

In line with the latter approach to microemulsification, the present work explores the formation and properties of nonaqueous SPC microemulsions, in which propylene glycol (PG) is employed

5

as the PS. PG is a widely utilised GRAS diol,[35] which, in addition to its behaviour as a solvent[33,35,36] and cosolvent,[37-41] can also act as a cosurfactant in systems stabilised by a variety of surfactants,[36,37,39-41] including PC lipids.[42-44] This ability of PG to partition into amphiphilic interfaces can influence both the formation of microemulsions (the partial[33,37,38] or complete[33,36,38] substitution of water with PG typically increases the range of compositions that form microemulsions) and their morphology (incorporation of PG commonly decreases the microemulsion droplets size[39,40,42]). PG's influence on microemulsification has been attributed to changes in a variety of interfacial properties, including an increase in the fluidity[36-38,41,45,46] and flexibility[37,38] of surfactant films, decrease in interfacial rigidity[37,41] and tension,[42,43,45,46] as well as changes in the interfacial curvature[37,38] and surfactant orientation.[43] As mentioned above, changes in some of these properties (especially the former three, all of which relate to a decrease in K)[27] are key to microemulsification in SPC-stabilised systems and, therefore, the use of PG as a PS offers notable advantages for the formulation of SPC microemulsions of improved toxicology. Nonetheless, the morphology of such nonaqueous microemulsions has not been investigated to date, which can hinder their future commercial applications and is a limitation, which we aim to address here.

Similarly to amphiphiles and PS, non-polar solvents (NPS) can also have a notable influence over the formation and morphology of microemulsions. To establish these effects, non-polar cyclic and acyclic hydrocarbons are commonly employed due to their systematically varying structure and properties,[21,28,47-49] while naturally derived NPS, such as soybean,[10,31,33] sunflower,[33] tea tree[41] and eucalyptus oil,[45] are increasingly utilised owing to their suitability for medicinal, dietary and cosmetic applications. Nevertheless, the poor biodegradability and/or toxicity[50] of hydrocarbons and the heterogeneous composition and/or chain length distribution of naturally derived NPS limit their applications to systematic studies of food- and drug-grade microemulsions. These limitations

have led to an increased utilisation of semi-synthetic NPS, such as fatty acids,[46,51] fatty acid esters[10-14,30,33,36,52] and mono-, di-, and triglyceride,[33,37,52] which offer the benefits of being both pharmaceutically acceptable and structurally homogeneous. Hence, in this work, eleven GRAS[53] fatty acid esters (FAE) with varying structural features (molecular volume, saturation and branching) were selected to investigate the effect of NPS structure and properties on the formation and morphology of pharmaceutically acceptable nonaqueous SPC-stabilised microemulsion.

As first postulated by *Schulman et al.* more than 60 years ago, the partition of NPS into the interfacial film of microemulsifying systems and the resulting changes in interfacial properties can also impact the formation of microemulsions.[54] A variety of hydrocarbon oils have been suggested to partition into the tail group area of SPC[21,28] and other PC lipids,[55] thereby altering their aggregation behaviour. Moreover, ^{13}C NMR spectroscopic studies of the vesicles formed by egg phosphatidylcholine (which is similar in structure to SPC) in the presence of FAE (*i.e.*, ethyl palmitate and ethyl oleate) have shown that in these low curvature systems the FAE partition not only into the surfactant tails region but also into the head group area of the PC lipids, as evidenced by the exposure of FAE carbonyl groups to the bulk solvent in the systems.[56] Previous studies have attributed this behaviour to the amphiphilic nature of FAE, which enhances their affinity for surfactant interfaces compared to that of non-amphiphilic oils, such as alkanes,[52] and promotes a FAE location and orientation in PC lipid interfaces akin to that of fatty acids (*i.e.*, with the FAE ester and hydrocarbon groups located in the PC lipid head and tail group areas, respectively).[51,56] The influence of NPS interfacial partition on the behaviour of microemulsifying systems is primarily guided by two factors. First, the extent of NPS incorporation into the surfactant monolayer has been associated with a range of NPS structural properties (such as molecular volume,[33,38,57] hydrophobic chain length,[3,29,38,55,58] aromaticity[57] and miscibility with the surfactant tails[38]) and has been suggested to exert a notable influence on C_0[25,58,59] and, hence, the preferred

microemulsion structure. Second, the structure of the partitioning NPS (*e.g.*, size,[29,49,55] saturation[60] and bulkiness[60]) has also been found to exhibit an effect on the elastic properties, such as K, of surfactant interfaces. Together, these factors govern the influence of NPS on the properties of microemulsifying systems, which we aim to study for the PG/SPC/FAE systems in this work.

To elucidate the influence of FAE on the behaviour of the nonaqueous systems we employed a complementary range of techniques, which provided information of the effect of FAE on microemulsification (phase behaviour studies), microemulsion droplet size (dynamic light scattering, DLS) and morphology (small-angle neutron scattering, SANS), as well as the extent of FAE interfacial partition (DLS and SANS) and the elastic properties of mixed SPC/FAE monolayers (Langmuir trough compression studies).

Experimental section

Materials. Propylene glycol (PG, Ph. Eur., water $\leq 0.2\%$), ethyl-*trans*-2 octenoate ($R_2R'_{8:1,t2}$, $\geq 98\%$), isoamyl caprylate ($R_{i-5}R'_{8:0}$, $\geq 98\%$), ethyl laurate ($R_2R'_{12:0}$, $\geq 98\%$), isoamyl laurate ($R_{i-5}R'_{12:0}$, $\geq 97\%$), isopropyl myristate ($R_{i-3}R'_{14:0}$, $\geq 98\%$), ethyl oleate ($R_2R'_{18:1,c9}$, Ph. Eur.), chloroform ($CHCl_3$, $> 99\%$) and ethanol ($> 99\%$) were purchased from Sigma-Aldrich. Methyl caprylate ($R_1R'_{8:0}$, 99%), ethyl caprylate ($R_2R'_{8:0}$, $\geq 98\%$), methyl laurate ($R_1R'_{12:0}$, 96%) and ethyl myristate ($R_2R'_{14:0}$, $\geq 98\%$) were obtained from Acros Organics and ethyl stearate ($R_2R'_{18:0}$, $\geq 95\%$) was acquired from Merck. 1,2-Propane-d_6-diol (d_6-PG, $> 98\%$, isotopic enrichment: 98%) and ethyl d_{15}-caprylate (d_{15}-$R_2R'_{8:0}$, $> 98\%$, isotopic enrichment: 98%) were purchased from C/D/N Isotopes. Soy L-α-phosphatidylcholine (SPC, 95%, fatty acid chain distribution: $C_{16:0}$ – 14.9 %, $C_{18:0}$ - 3.7 %, $C_{18:1}$ – 11.4 %, $C_{18:2}$ – 63.0 %, and $C_{18:3}$ – 5.7 %), 1-palmitoyl-2-oleoyl-*sn*-glycero-3-phosphocholine (POPC, $> 99\%$) and 1-palmitoyl-d_{31}-2-oleoyl-*sn*-glycero-3-phosphocholine (d_{31}-POPC, $> 99\%$) were acquired form Avanti Polar Lipids. Water was obtained from an ELGA Purelab water purification system. All materials were used without further purification.

Phase behaviour. Partial ternary and pseudo-ternary phase diagrams of PG/SPC/FAE systems containing one or two FAE, respectively, were constructed using a titration method at room temperature (RT, 23 ± 2 °C). For this purpose, PG/SPC and FAE/SPC mixtures, in which the concentration of SPC ranged between 2.5 and 40 % w/w, were prepared and allowed to mix overnight. The PG/SPC and FAE/SPC mixtures were then titrated under constant stirring with a FAE or PG, respectively. The turbidity and birefringence of the systems were assessed by visual inspection through cross-polaroids (P.W Allen & Co.) prior to and during titration to determine the boundaries between the different phases. Mixtures that were single-phased, non-turbid and non-birefringent were classified as potential microemulsions, while cloudy, non-birefringent

mixtures were classified as non-microemulsion phases and were not investigated further. No birefringent mixtures were obtained prior to or during titration. The appearance of the mixtures remained unchanged for one year at RT.

Partial phase diagrams for the PG/SPC/FAE systems were plotted on ternary plots, where each corner represents the weight of one or a mixture of components, *i.e.*, PG, SPC or FAE, as a percentage of the total sample weight (% w/w). The area of potential microemulsion existence was determined as a percentage of the total phase diagram area studied using the image processing software ImageJ.[61] The sizes of the non-turbid, non-birefringent phase diagram areas were observed to increase with an increase in experimental temperature (*cf.* Supporting Material) but these changes were not significant in the range of laboratory temperature fluctuations (± 2 °C) and where more than one phase diagram was obtained at RT (23 ± 2 °C) for a given protiated system the phase boundary agreement was excellent.

Dynamic light scattering (DLS). The average size (apparent radius of solvation, R_S) and size distribution (polydispersity index, PDI) of one-phase non-turbid non-birefringent PG/SPC/FAE samples was measured in triplicate at 25 and/or 37 °C using a Zetasizer Nano ZS (Malvern Instruments Ltd.). For this purpose, PG-continuous PG/SPC/FAE samples with SPC concentration of 2.5, 5 or 10% w/w and FAE concentration between 0 and 16 % w/w were prepared and allowed to mix overnight.

For the measurements, the samples were transferred to polystyrene cuvettes and allowed to equilibrate at the measurement temperature for at least 10 minutes. The emission wavelength of the He-Ne laser was 633 nm and the measurement angle was 173°. The refractive index of the dispersant (continuous phase, PG) was specified as 1.432[35] and its viscosity was determined using a dynamic strain-controlled rheometer (ARES, TA instruments Co.) coupled to a Peltier

temperature controlling unit and fitted with a titanium plate (50 mm diameter). The viscosity of PG was recorded as 40.9 ± 0.7 cP at 25 °C and 23.1 ± 0.4 cP at 37 °C, which agreed well with literature values.[62]

Measurements data were processed using the Malvern Zetasizer software, which uses the Stokes-Einstein equation to determine the hydrodynamic radius (R_H) of spherical particles as:

$$R_H = \frac{k_B T}{6\pi\eta D}$$

where k_B is the Bolzmann constant, T is the temperature, η is the viscosity of the dispersant and D is the diffusion coefficient of the dispersed particles. As the nanostructures in analogous d_{31}-POPC-stabilised systems were determined by small-angle neutron scattering (SANS) not to be spherical (see Results and discussion), the apparent hydrodynamic radii were used to qualitatively assess trends in the size of aggregates and correlate them with results from SANS. The standard deviation (SD) of the apparent R_S was calculated as: $SD = R_S \sqrt{PDI}$ in agreement with the recommendations by the manufacturer of the DLS equipment.

Small-angle neutron scattering (SANS). The morphology of the structures in PS-continuous samples employing PG or d_6-PG as the PS, POPC or d_{31}-POPC as the surfactant and $R_2R'_{8:0}$, d_{15}-$R_2R'_{8:0}$, $R_2R'_{12:0}$ or $R_2R'_{18:1,c9}$ as the FAE was studied using SANS. The selected $(d_6$-)PG/(d_{31}-)POPC/FAE samples had a (d_{31}-)POPC concentration of 5% w/w and FAE concentration between 0 and 10% w/w (concentrations of deuterated components were adjusted to preserve component mol ratios between equivalent samples of varying isotropic contrast). All samples were allowed to mix overnight after preparation.

For the SANS measurements, the solutions were transferred to 1 mm path length quartz cells and their scattering was measured at 37 °C at the SANS2D beam line (STFC ISIS facility). The

detectors were positioned at a sample-to-detector distance of 2.4 m and 4.0 m to cover a scattering vector, Q, range of 0.005−1.7 Å^{-1}. The data obtained were normalized for detector response and spectral distribution of the incident beam, averaged radially and over the collection time and adjusted for the scattering of the bulk solvent (PG or d$_6$-PG). This resulted in one dimensional plots of the variation in scattering intensity, $I(Q)$, with Q, *i.e.*, scattering curves. Additionally, in data where the solvent was over subtracted, the affected scattering curve was manually adjusted by assuming a flat background and adding a constant, small value to all the data.

The scattering curves were analysed using the small-angle scattering analysis software package SasView.[63] All (d$_6$-)PG/(d$_{31}$-)POPC(/FAE) nanostructures were assumed to be non-interacting at the surfactant concentrations employed (5% w/w) and, hence, the structure factor ($S(Q)$) was neglected in the data modelling by setting it to 1. The SLD of the systems' components were calculated using SasView's SLD calculator (*cf.* Table S1).[63] A volume-weighted average of the SLD of the FAE and (d$_{31}$-)POPC tails group was used as the nanostructures' effective SLD and fixed (Table S2). Additional small scattering objects detected in the high Q region were modelled using the SLD of the deuterated hydrocarbon chain of d$_{31}$-POPC (for d$_{31}$-POPC-stabilised systems) or the SLD of the POPC molecule (for POPC-stabilised systems) (Table S2). All assumptions made during data analysis are discussed in the Results and discussion section.

Model-fitting of the SANS data for (d$_6$-)PG/(d$_{31}$-)POPC(/FAE) systems was performed using the sum of a triaxial ellipsoidal model (for the (d$_{31}$-)POPC(/FAE) nanostructures) and a spherical model (for the small lipid structures). The polydispersity of both morphologies was set at 0% to reduce the computational demand of the fitting calculations. Although microemulsions are reported to have a characteristic low polydispersity owing to their molecular packing,[3] this fixed polydispersity could introduce an error in the reported values. The SANS profiles of samples of equivalent composition but different isotopic make-up (contrast) were fitted independently.

Langmuir trough (LT) monolayer studies. The behaviour of SPC (and one or two FAE) at the air-water interface at RT (23 ± 2 °C) was examined using LT monolayer compression experiments. Prior to each measurement all equipment was cleaned with ethanol and chloroform ($CHCl_3$) and all glassware was repeatedly rinsed with ethanol and purified water. For the measurements, SPC (1 mg/ml) or an equimolar mixture of SPC (1 mg/ml) and FAE ($0.2 - 0.4$ mg/ml) was dissolved in $CHCl_3$. The LT (Nima Technologies Ltd., UK, enclosed in a protective box) was filled with ultra-pure water and the water surface was cleaned using a vacuum pump until the recorded surface pressure (π) was constant (maximum variation of ± 0.2 mN/m^2 upon compression). Between 25 and 45 µl of the SPC(/FAE)/CHCl$_3$ solution was deposited on the water surface using a 50 µl syringe (Hamilton Co. Europe, Switzerland). Thirty minutes were allowed for CHCl$_3$ to evaporate and the SPC(/FAE) monolayer to equilibrate. Subsequently, the monolayer was compressed at a speed of 35 cm^2/min from the initial air/water interfacial area (A_{AW}) of 495 cm^2 to a final A_{AW} of 80 cm^2. The changes in π upon compression were recorded using a surface pressure microbalance (Nima Technologies Ltd., UK) fitted with a Wilhelmy plate (Whatman Grade 1 chromatographic paper, GE Healthcare life sciences UK, UK). Each SPC(/FAE)/CHCl$_3$ composition was prepared at least in duplicate and measured at least in duplicate (n = 4-7).

For the analysis, the SPC and FAE molecules were assumed to be homogeneously mixed and the molecular weight of SPC/FAE complexes (Mw_c) was calculated as:

$$Mw_c = \sum_{i=1}^{n} \frac{Mw_i n_i}{n} \times N_{SA},$$

where Mw_i and n_i are the molecular weight and number of moles of the *i*-th surface-active component, respectively, *n* is the total number of moles of surface-active components and N_{SA} is the number of surface-active components.[64] A_{AW} was then converted to area per SPC(/FAE) complex (A_c) using the equation:

$$A_c = \frac{A_{AW} \, Mw_c}{c_c \, V_c},$$

where c_c is the sum of the concentrations of all surface-active species and V_c is the volume of deposited SPC(/FAE)/CHCl$_3$ solution. The recorded π was plotted against the calculated A_c to obtain surface pressure-area per complex, π-A_c, isotherms. All isotherms for systems of equivalent composition were averaged in the software Origin (OriginLab, USA). The limiting surface area per complex for each SPC(/FAE) systems ($A_{c,lim}$) was obtained by extrapolating the isotherm region of highest $d\pi/dA_c$ slope to $\pi = 0$ mN/m^2.[64,65] The monolayer collapse pressure (π_{coll}) was determined as the point of sharpest $d\pi/dA_c$ slope change.[66]

The compressibility modulus (C_s^{-1}) of the monolayers was calculated as:[65]
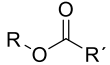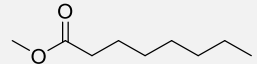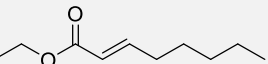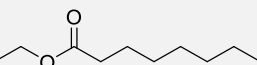
$$C_s^{-1} = -A_c \frac{d\pi}{dA_c}$$
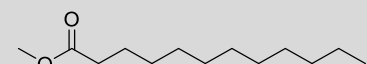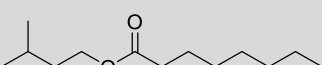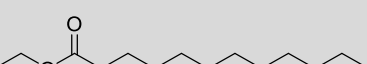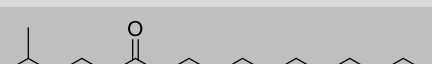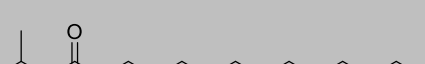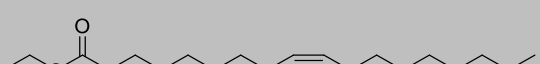
The calculated C_s^{-1} was plotted against the recorded π to obtain compressibility curves. All compressibility curves for systems of equivalent composition were averaged in Origin. The maximum compressibility modulus value ($C_s^{-1}{}_{max}$) for each compressibility curve was identified.

Statistical data analysis. Statistical data analysis was performed using a one-way ANOVA test in SigmaPlot 14 with p < 0.05 considered significant.

Results and discussion

Overview of selected fatty acid esters. Eleven fatty acid esters (FAE) of varying structural features (molecular volume, saturation and branching) were selected for the studies in this work (Table 1). The FAE have a molecular volume (MV) between 299 and 611 Å^3 and comprise one of four parent alcohol groups (R) of varying branching (linear or branched) and one of six parent fatty acid groups (R′) of varying saturation (saturated, *trans*-monounsaturated, *cis*-monounsaturated), which are linked *via* an ester group (Table 1). The influence of FAE structure on the behaviour of soybean phosphatidylcholine (SPC)-stabilised systems was investigated in ternary propylene glycol (PG)/SPC/FAE or binary SPC/FAE mixtures, except for the FAE ethyl stearate ($R_2R'_{18:0}$), which is solid at room temperature and, therefore, was employed in a 1:1 weight ratio with a structurally similar FAE, *i.e.*, ethyl oleate ($R_2R'_{18:1,c9}$), in quaternary PG/SPC/$R_2R'_{18:0}$/$R_2R'_{18:1,c9}$ and ternary SPC/$R_2R'_{18:0}$/$R_2R'_{18:1,c9}$ mixtures, respectively. Some low molecular volume FAE, such as ethyl caprylate ($R_2R'_{8:0}$), are slightly soluble in PG (solubility < 1 % w/w),[67] which could have a small but statistically significant effect on the phase behaviour and structural data reported. Additionally, while the systems studied throughout this work are referred to as nonaqueous and great care was taken to limit the exposure of the individual components and their mixtures to water and air, it is likely that trace amounts of water are present in them. Here, we examine the experimental results obtained without considering the effect of trace water in the systems.

Table 1. Molecular volume, branching and saturation of fatty acid esters (FAE) and size of non-turbid, non-birefringent (potential microemulsion) areas in corresponding PG/SPC/FAE phase diagrams. FAE names are abbreviated according to the chain length and branching of the parent alcohol (R) group (R_1 – methyl, R_2 – ethyl, R_{i-3} – isopropyl, R_{i-5} – isoamyl) and the chain length and saturation (unsaturated bond geometry and position) of the parent fatty acid (R′) group ($R'_{8:0}$ – caprylic, $R'_{8:1,t2}$ – *trans*-2-octenoic, $R'_{12:0}$ – lauric, $R'_{14:0}$ – myristic, $R'_{18:0}$ – stearic, $R'_{18:1,c9}$ – oleic (cis-9)). FAE are shaded in light, medium and dark grey according to the grouping in which they are presented in Figure 1, 2 and 4, *i.e.*, A, B and C, respectively.

Name and abbreviation	Chemical structure	Molecular volume ($Å^3$)[a]	Branched R groups/ Unsaturation in R′ groups	Size of non-turbid non-birefringent phase diagram area (%)
General FAE structure				
Methyl caprylate ($R_1R'_{8:0}$)		299	-/-	77
Ethyl octenoate ($R_2R'_{8:1,t2}$)		320	-/trans-mono-unsaturation	71
Ethyl caprylate ($R_2R'_{8:0}$)		330	-/-	64
Methyl laurate ($R_1R'_{12:0}$)		409	-/-	45
Isoamyl caprylate ($R_{i-5}R'_{8:0}$)		413	1/-	48
Ethyl laurate ($R_2R'_{12:0}$)		440	-/-	45
Ethyl myristate ($R_2R'_{14:0}$)		495	-/-	45
Isoamyl laurate ($R_{i-5}R'_{12:0}$)		525	1/-	48
Isopropyl myristate ($R_{i-3}R'_{14:0}$)		528	1/-	49
Ethyl oleate ($R_2R'_{18:1,c9}$)		593	-/cis-mono-unsaturation	49
Ethyl stearate ($R_2R'_{18:0}$)		611	-/-	47[b]

[a] The molecular volume of the FAE was calculated using the manufacturer specified molecular weight and density.

[b] The effect of ethyl stearate on phase behaviour was studied in a PG/SPC/FAE system, in which the FAE was a mixture of ethyl stearate and ethyl oleate of a 1:1 weight ratio.

Phase behaviour. The phase behaviour of eleven PG/SPC/FAE systems employing the FAE shown in Table 1 was investigated at room temperature (Figure 1). Studies were limited to SPC concentrations below 40% w/w (*ca.* 55% of the phase diagram area), as low-to mid-surfactant concentration are typically favoured in food and drug formulations due to cost and biocompatibility considerations.[15] The focus in the description of the results is on the one-phase, clear, non-birefringent phase diagram area, as it likely corresponds to a microemulsion phase (as confirmed by the structural studies that follow). The size of the potential microemulsion area in the phase diagram region investigated varied between 45 and 77% (Table 1) and its relationships to the properties of the polar solvent (PS) and non-polar solvent (NPS) in the systems are discussed below. The effect of temperature on the size of the potential microemulsion area is briefly discussed in Supporting Material. All discussed trends are also valid when expressing component concentrations in mol/mol percentages (% mol/mol, Figure S1).

Effect of polar solvent. The effect of employing a nonaqueous PS, *i.e.*, PG, instead of water on the phase behaviour of PS/SPC/FAE systems is examined first. For this purpose, the phase behaviour of PG/SPC/FAE systems reported in this study (Figure 1) was compared to that previously obtained elsewhere for water/SPC/FAE systems employing isopropyl myristate $(R_{i-3}R'_{14:0})$[11-14] or $R_2R'_{18:1,c9}$[10] as the FAE and an additional amphiphile. The results suggest that the phase behaviour of aqueous and nonaqueous PS/SPC/FAE systems differs in three distinct ways. First, the PG/SPC/FAE systems formed relatively large potential microemulsion regions and no liquid crystalline (LC) or gel areas in their partial phase diagrams (Figure 1), while water/SPC/FAE systems were reported to form microemulsion phases (typically accompanied by a LC[10,12,13] or gel[11] area of existence) only in the presence of an additional amphiphile, *i.e.*, a surfactant[11] or co-surfactant.[10,12-14] Second, the potential microemulsion region in all partial PG/SPC/FAE phase diagrams is continuous and extends over both PS-rich and NPS-rich compositions (Figure 1),

17

whereas aqueous SPC-stabilised systems often form large microemulsion phase diagram areas at high NPS concentrations[10,12,13] and only small ones at high aqueous concentration - a region dominated instead by birefringent and turbid phases.[10,12-14] Third, the formation of clear non-birefringent phases in PG/SPC/FAE systems is observed at relatively low SPC concentrations (~ 2% w/w, *i.e.*, the lowest SPC concentrations studied, Figure 1), while microemulsification in water/SPC/FAE systems is commonly observed at SPC concentrations higher than 5 % w/w[12,14] or 10% w/w.[10,11]

The observed differences between the phase behaviour of aqueous and nonaqueous SPC-stabilised systems compare well with previous studies, which report that the incorporation of PG in systems stabilised by various surfactants, including SPC[33] and POPC,[42] is correlated with an increase in the area of microemulsion existence[33,36-38,41,42,45,46] and, when applicable, a decrease in the areas of LC[33,36-38,42] or gel[45,46] phase formation in phase diagrams. As discussed in the Introduction, these phase behaviour differences are commonly attributed to the ability of PG to act as a cosurfactant[36,37,39-44] and, thereby, alter the interfacial properties of microemulsifying systems. Specifically, the use of PG has previously been suggested to decrease the bending elastic constant, K,[37,41] (or, relatedly,[27] increase the interfacial fluidity[36-38,41,45,46] and/or flexibility[37,38]) and modify the preferred curvature, C_0,[37,38] of interfacial films. Therefore, we hypothesise that in our nonaqueous SPC-stabilised systems PG also likely acts as a cosurfactant, thereby modifying C_0, lowering K and allowing the formation of microemulsions over an extended range of compositions. This hypothesis is discussed further in the following sections describing the size and morphology of the aggregates.
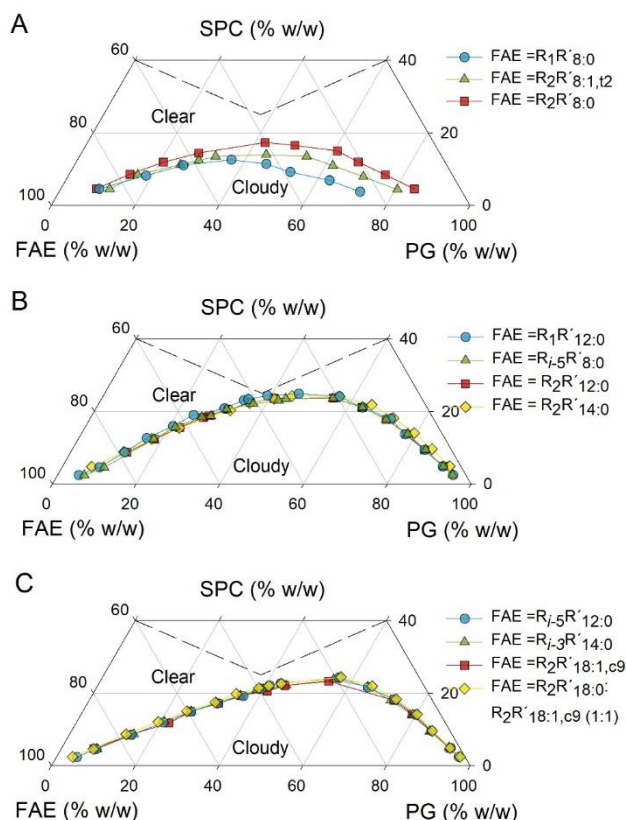
Figure 1. Partial phase behaviour of PG/SPC/FAE systems employing the following FAE in order of increasing molecular volume: (A) methyl caprylate ($R_1R'_{8:0}$, ●), ethyl octenoate ($R_2R'_{8:1,t2}$, ▲), ethyl caprylate ($R_2R'_{8:0}$, ■); (B) methyl laurate ($R_1R'_{12:0}$, ●), isoamyl caprylate ($R_{i-5}R'_{8:0}$, ▲), ethyl laurate ($R_2R'_{12:0}$, ■), ethyl myristate ($R_2R'_{14:0}$, ◆); (C) isoamyl laurate ($R_{i-5}R'_{12:0}$, ●), isopropyl myristate ($R_{i-3}R'_{14:0}$, ▲), ethyl oleate ($R_2R'_{18:1,c9}$, ■), ethyl stearate:ethyl oleate (1:1) ($R_2R'_{18:0}$:$R_2R'_{18:1,c9}$ (1:1), ◆). Dashed lines in all phase diagrams delimit the investigated region. Clear phases were single-phased; cloudy phases separated upon standing; both phases were non-birefringent. All component concentrations are expressed as component weight/total sample weight percentages (% w/w).

Effect of fatty acid ester molecular volume. The effect of the FAE structural properties, *i.e.*, molecular volume (MV), R′ saturation and R branching, on the formation of potential microemulsions is examined next, starting with the FAE MV. The phase behaviour results suggest that an increase in FAE MV from 299 Å^3 (methyl caprylate, $R_1R'_{8:0}$) to 409 Å^3 (methyl laurate, $R_1R'_{12:0}$) is correlated with a reduction in the size of the potential microemulsion area of existence

19

from 77 to 45% (Table 1, Figure 1 (A, B)). This reduction is notably stronger for PG-rich mixtures, which are expected to have an oil-in-PG (equivalent to oil-in-water) droplet structure and a positive spontaneous curvature, C_0. Interestingly, an increase in FAE MV beyond this value (*ca.* 409 Å^3) is not associated with a further reduction in the clear area of PG/SPC/FAE phase diagrams. In particular, all systems employing FAE of molecular volume between 409 Å^3 (methyl laurate, $R_1R'_{12:0}$) and 611 Å^3 ($R_2R'_{18:0}$:$R_2R'_{18:1,c9}$ (1:1)) produced phase diagrams with a clear area between 45 and 49% (Table 1, Figure 1 (B, C)).

To provide a speculative explanation for the observed effect of FAE MV on phase behaviour, the two key factors guiding the influence of NPS on microemulsification (presented in the Introduction) were utilised. First, an increase in NPS size (typically expressed as MV[33,38,57] and/or hydrophobic chain length[3,29,38,55]) has commonly been correlated with a decrease in the extent of NPS partition into the interface of microemulsifying systems. Additionally, as discussed in the Introduction, FAE have an amphiphilic structure, which may support their partition into both the tail and head group regions of PC lipids,[56] thereby potentially affecting the lipids' interfacial packing and curvature in a similar manner to that of other small-to-medium amphiphiles. Specifically, previous studies have reported that the incorporation of smaller amphiphiles into monolayers composed of larger ones is associated with an increase in C_0, the magnitude of which increases with the smaller amphiphile concentration.[68] Therefore, we suggest that an increase in FAE MV is correlated with a decrease in their interfacial partition and, hence, a decrease in C_0. This suggestion is supported by the partial phase diagrams of systems employing FAE with MV between 299 Å^3 to 409 Å^3 (Figure 1 (A, B)), for which an increase in FAE MV is associated with a notable decrease in the formation of potential microemulsions of positive C_0 – a correlation which would be expected for the proposed changes in C_0 with FAE MV. This hypothesis will be examined further with dynamic light scattering (DLS) and small-angle neutron scattering (SANS).

Second, previous studies have correlated an increase in NPS MV with a decrease in the monolayer rigidity of microemulsions (expressed as K[29,49,69] or $2K + \overline{K}$,[55] where $\overline{K}$ is the Gaussian elastic modulus) using a range of techniques, *i.e.*, tensiometry,[29,49,55,69] ellipsometry[29,49,69] and scattering[55] experiments. As discussed in the Introduction, a decrease in K is a prerequisite for microemulsion formation in SPC-stabilised systems. Moreover, according to the film bending model developed by *Helfrich*,[70] it would also result in a decrease in the film bending free energy (F) of an amphiphile(s) layer, which is described as $F = \frac{1}{2}K(C_1 + C_2 - 2C_o)^2 + \overline{K}C_1C_2$, where C_1 and C_2 are the two principal interfacial curvatures in the x and y direction, which can be averaged to obtain the mean interfacial curvature, C.[70] Based on the relationship above, this, in turn, would increase the range of principal interfacial curvatures supporting a thermodynamically favourable formation of microemulsions and, hence, also increase the overall area of microemulsion formation. This relationship between FAE MV and monolayer elastic properties is discussed in our SANS and Langmuir trough (LT) monolayer compression studies. Combining the considerations above, we suggest that an increase in NPS MV can both decrease C_0 (thereby decreasing the range of oil-in-PG microemulsion forming compositions) and decrease K (thereby increasing the range of compositions that support microemulsification). Together, these two opposing effects can provide a speculative explanation for the relatively small differences in the potential microemulsion phase diagram area observed for PG/SPC/FAE systems employing FAE of MV between 409 Å^3 and 611 Å^3 in this work (Figure 1 (B, C)).

Effect of fatty acid ester saturation. The effect of FAE R′ group saturation on the size of the clear non-birefringent region in partial PG/SPC/FAE phase diagrams was assessed next. For this purpose, the phase behaviour of systems employing saturated or unsaturated FAE of similar MV was compared in pairs (Figure S2). The results suggest that the potential microemulsion area increases with decreasing FAE saturation. This change is significant (7%) when comparing the

areas of potential microemulsion formation for systems containing ethyl octenoate ($R_2R'_{8:1,t2}$) or ethyl caprylate ($R_2R'_{8:0}$) and only marginal (2%) when comparing systems containing $R_2R'_{18:1,c9}$ or the mixture of $R_2R'_{18:0}$ and $R_2R'_{18:1,c9}$ in a 1:1 weight ratio (Table 1, Figure S2).

The results agree well with recent studies of water/SPC/fatty acid (FA) systems comprising either saturated (palmitic acid), mono-unsaturated (oleic acid) or di-unsaturated (linoleic acid) FA, which report that increasing the degree of FA saturation destabilizes the formation of lamellar phases and instead promotes the existence of hexagonal, cubic, micellar and microemulsion phases.[51] The authors attributed the inverse relationship between NPS saturation and the formation of clear, isotropic, non-birefringent phases to the improved mixing between the unsaturated phospholipid tails of SPC and unsaturated NPS.[51] Hence, we also hypothesise that an improved mixing between the SPC tails and unsaturated FAE is responsible for the observed increase in the phase diagram area of microemulsion existence (Table 1, Figure S2). Nonetheless, the effect of FAE saturation appears to be relatively weak and, indeed, insignificant to both the bulk and interfacial properties of the systems studied in the next sections. This was attributed to a combination of two factors. First, both unsaturated FAE in this work were monounsatured and previous studies of the influence of tails saturation suggest that changes in PC lipid interfacial behaviour are stronger when polyunsaturation is introduced compared to monounsaturation.[71] Second, the selection of FAE employed included only two unsaturated FAE (Table 1), which also limits the scope of the conclusions that can be drawn about the effect of saturation.

Effect of fatty acid ester branching. Finally, the effect of FAE R group branching on the formation of potential microemulsions in PG/SPC/FAE systems was considered. To facilitate this assessment the phase behaviour of systems employing linear or branched FAE of similar MV was compared in pairs (Figure S3). The results suggest that the use of branched FAE, *i.e.*, isoamyl caprylate ($R_{i-5}R'_{8:0}$), isoamyl laurate ($R_{i-5}R'_{12:0}$) or $R_{i-3}R'_{14:0}$, is associated with a small but

consistent increase in the potential microemulsion phase diagram area (3 - 4%) compared to systems employing linear FAE of similar MV, *i.e.*, methyl laurate ($R_1R'_{12:0}$) or ethyl myristate ($R_2R'_{14:0}$) (Table 1, Figure S3).

A possible interpretation of the observed effect of FAE R group branching on PG/SPC/FAE phase behaviour is provided below. As discussed in the Introduction, FAE have been suggested to partition into PC lipid structures in a manner akin to that of other amphiphiles, such as fatty acids,[56] thereby affecting the interfacial properties and microemulsification of the systems in a comparable way. In the literature, comprehensive studies of the effect of amphiphile branching on phase behaviour have commonly focussed on surfactants and cosurfactants. For instance, *Ezrahi et al.* studied the effect of a wide range of alcohols on the phase behaviour of systems stabilised by a variety of surfactants.[72,73] The authors suggest that an increase in the branching of the amphiphile(s) present at the PS/NPS interface correlates with a reduction in the intermolecular cohesive forces in the interfacial layer, which, in turn, promotes the formation of structures with a more disordered interface, such as microemulsions, over structures with a high degree of order, such as liquid crystals.[72,73] The results presented here are broadly consistent with these correlations and, therefore, we suggest that the influence of branched FAE on the SPC monolayer is comparable. Nonetheless, the effect of FAE branching on the phase behaviour of PG/SPC/FAE systems is notably weak and no overarching conclusions can be drawn from the limited number of systems studied here. Moreover, changes in FAE R group branching were not associated with any significant changes in the bulk and interfacial properties of the systems studied in the following sections.

Overall, our phase behaviour results suggest that the use of PG as a PS in SPC-stabilised systems supports the existence of clear, one-phase mixtures over an extended range of compositions. Furthermore, they reveal that the size of the area of microemulsion formation in PG/SPC/FAE

systems is also variously affected by the molecular volume, saturation and branching of FAE, with the latter two having a marginal effect. These changes were attributed to the partition of FAE in the interfacial layer of the microemulsifying systems and the resulting changes in its curvature and elasticity properties, among others. The phase behaviour differences, while relatively small and determined from a limited set of FAE structures, are consistent across this range of FAE and concur with previous studies. Next, we examine the size (dynamic light scattering, DLS) and morphology (small-angle neutron scattering, SANS) of the self-assembled structures.

Size of the self-assembled structures by dynamic light scattering (DLS). To gain further understanding of the effect of FAE molecular structure on the behaviour of nonaqueous SPC-stabilised systems, the size of the self-assembled structures in PG/SPC/FAE mixtures was examined using DLS. The selected compositions encompass PS-rich mixtures of SPC (2.5, 5 or 10 % w/w) and FAE (0 - 16% w/w, varied in two-fold increments), which were identified to be single-phased, non-turbid and non-birefringent (potential microemulsions, Figure 1) and are potentially suitable for drug and food applications due to their low surfactant and oil content.[15] DLS measurements were carried out at 25 °C for PG/SPC/FAE mixtures comprising each of the eleven FAE shown in Table 1, while a smaller selection of systems was also studied at 37 °C to aid comparison with small-angle neutron scattering data collected at the same temperature and discussed in the following section.
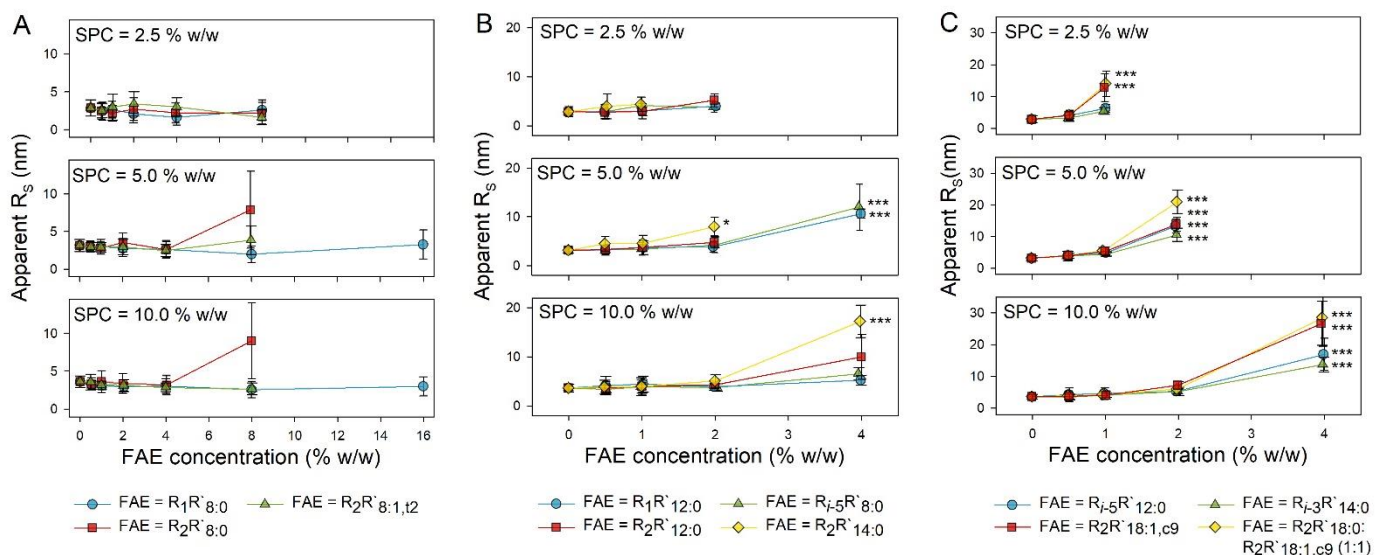
Figure 2. Average apparent radius of solvation (R_S) of aggregates in PG/SPC/FAE systems at 25 °C employing the following FAE in order of increasing molecular volume: (A) methyl caprylate ($R_1R'_{8:0}$, ●), ethyl octenoate ($R_2R'_{8:1,t2}$, ▲), ethyl caprylate ($R_2R'_{8:0}$, ■); (B) methyl laurate ($R_1R'_{12:0}$, ●), isoamyl caprylate ($R_{i-5}R'_{8:0}$, ▲), ethyl laurate ($R_2R'_{12:0}$, ■), ethyl myristate ($R_2R'_{14:0}$, ◆); (C) isoamyl laurate ($R_{i-5}R'_{12:0}$, ●), isopropyl myristate ($R_{i-3}R'_{14:0}$, ▲), ethyl oleate ($R_2R'_{18:1,c9}$, ■), ethyl stearate:ethyl oleate (1:1) ($R_2R'_{18:0}$:$R_2R'_{18:1,c9}$ (1:1), ◆). Samples were prepared in singlicates and measurements were obtained in triplicates. Standard deviations (SD) were calculated using the samples' polydispersity index (PDI) as: $SD = R_S \sqrt{PDI}$. The statistical significance of the size differences between PG/SPC and PG/SPC/FAE nanostructures of equivalent SPC concentration are shown ($p < 0.05$ (*), $p < 0.001$ (***)).

The results of the DLS measurements at 25 °C reveal that the self-assembled structures in PG/SPC(/FAE) mixtures have an apparent R_S between 1.6 nm and 28.5 nm and an average PDI of 0.12 ± 0.09 (Figure 2). To gauge the stability of the nanostructures, the size of each sample was recorded one year after the initial measurement and the change in apparent R_S over the period was calculated as a percentage of the initially recorded particle size. The nanostructures showed good stability over the period with their apparent R_S changing by $12 \pm 15\%$ on average (data not shown). The effects of sample composition, *i.e.*, PS type, dispersed phase (SPC and FAE) concentration and FAE molecular structure, on the size of the self-assembled structures at 25 °C were assessed independently and are discussed below. The effect of temperature (25 °C or 37 °C) on the apparent R_S of aggregates in samples of equivalent composition is also briefly discussed in Supporting Material.

Effect of polar solvent. The effect of employing PG instead of water as the PS on the apparent R_S of self-assembled structures in PS-rich SPC-stabilised systems at 25 °C was evaluated first. For this purpose, the DLS data obtained here for PG/SPC/$R_{i\text{-}3}R'_{14:0}$ mixtures (Figure 2 (C)) was compared to that reported elsewhere for water/SPC/$R_{i\text{-}3}R'_{14:0}$ mixtures of similar SPC concentration (3.6 – 11 % w/w) and slightly higher FAE concentration (5 – 12 % w/w).[11,14] The comparison suggests that, depending on the additional amphiphile used to promote microemulsification, *i.e.* polysorbate[11] or ethanol,[14] the radii of the structures in the aqueous systems are slightly larger (between ~10 and ~25 nm) or comparable (between ~2.5 and ~4.5 nm) to those in the nonaqueous systems (between 2.9 and 13.7 nm), respectively.

Before discussing these results, it should be noted that conclusions from the above comparison are limited both by the unavailability of data for ternary oil-in-water water/SPC/FAE systems (as discussed above, such systems do not readily form microemulsions unless an additional amphiphile is used) and by the small number of aqueous SPC-stabilised microemulsions previously

26

characterised using DLS. Nevertheless, the comparison suggests that the use of PG in PS-rich SPC-stabilised systems brings about a reduction in the size of the self-assembled structures (when compared to systems comprising an additional surfactant, *i.e.*, polysorbate[11]) to radii similar to those obtained in cosurfactant-containing systems (*i.e.,* water/ethanol/SPC/R$_{i\text{-}3}$R′$_{14:0}$).[14] These observations are in good agreement with previous reports of a reduction in microemulsion droplets size upon PG addition[39,40,42] and support our hypothesis that the influence of PG on microemulsification is akin to that of cosurfactants. Hence, we speculate that these observations can be attributed to the ability of PG to partition into the interfacial layer of PG/SPC/FAE systems, thereby, altering its bending elastic constant, K,[37,41] and preferred curvature, C_0,[37,38] and, thus, also the radii of the microemulsion droplets.[3,27]

Effect of dispersed phase concentration. Next, the influence of SPC and FAE concentration on the apparent R_S of the structures is assessed. Previous studies have suggested that the effect of component concentration on the size of microemulsion droplets is primarily guided by the component localisation in the aggregates.[57] In particular, an increase in the concentration of components at the microemulsion interface is expected to increase the droplets' surface-to-volume ratio (A/V) and, hence, decrease their average radius ($r \sim \frac{1}{A/V}$), while an increase in the concentration of components in the microemulsion core is expected to have the opposite effect.[57]

Based on the geometric relationship outlined, the effect of SPC concentration of on the apparent R_S of the structures is examined first. To facilitate the assessment, mixtures comprising FAE of equivalent concentration were compared (Figure S4). The comparison suggests that an increase in SPC content (between 2.5 and 10 % w/w) is generally associated with a marginal decrease in the size of the self-assembled structures (Figure S4). As outlined in the geometric relationships above, this result is indicative of an increase in the concentration of components at the microemulsion droplets' interface which suggests that SPC indeed acts as a surfactant in the systems.

Next, the influence of FAE concentration on the aggregates' size is assessed. Generally, the apparent R_S of nanostructures within a PG/SPC/FAE sample set (*i.e.*, set of samples comprising the same FAE type and SPC concentrations) increases with FAE concentration (Figure 2). In line with published DLS studies of microemulsions,[74] this relationship can be used as a confirmation of FAE incorporation into the self-assembled structures, thereby supporting the proposed self-assembly structure for the nonaqueous mixtures¸ *i.e.*, that of microemulsion droplets. Furthermore, according to the geometric relationship outlined above, the correlation between FAE concentration and apparent R_S also suggests that at least some FAE contribute to the formation of a microemulsion core.

Interestingly, this positive correlation between microemulsion droplet radius and FAE concentration becomes notably more pronounced as the FAE concentration increases. In particular, the apparent R_S of microemulsions comprising the highest FAE concentration within a sample set is often significantly larger than that of the FAE-free micelles of equivalent SPC concentration, while aggregates comprising lower FAE concentrations are only marginally different to the corresponding micelles (Figure 2). A possible explanation for these observations can be provided on the basis of the above geometric correlations and the suggested location of FAE molecules, *i.e.*, both in the microemulsion core (discussed above) and in the PC lipid monolayer (in agreement with literature).[56] In particular, we propose that the ratio of FAE molecules that partition in the interfacial layer *vs.* those contained in the microemulsion core decreases as the FAE concentration increases; which, in turn, leads to small droplet size changes at low FAE concentration (for which a larger fraction of FAE molecules reside at the interface) and often significant droplet size growth at the highest FAE concentrations (for which a comparably larger fraction of FAE molecules reside in the microemulsion core) within each sample set (Figure 2). The proposition that oil partition into PC lipid structures is oil concentration-dependent is in agreement with previous studies of

28

alkane partition into egg PC lipid bilayers, which report a decrease in the fraction of bilayer-partitioning alkane molecules as the alkane concentration increases beyond a specific threshold.[75]

Both of the relationships discussed above become more pronounced as the FAE MV increases, *i.e.*, the influence of SPC concentration on the microemulsions' size becomes stronger (Figure S4) and the growth in apparent R_S with FAE concentration becomes larger (Figure 2). Therefore, we focus on the effect of FAE MV on the size of the microemulsions next.

Effect of fatty acid ester structural properties. The influence of FAE structure (Table 1) on the apparent R_S of the microemulsion droplets is examined next. First, changes in FAE branching and saturation were not associated with significant changes in microemulsion droplet size (likely due to the limited number of branched or unsaturated FAE studied and in agreement with our phase behaviour studies). Next, the influence of FAE MV on the aggregates' size was examined by plotting the apparent R_S *vs.* FAE MV for samples of equivalent SPC and FAE concentration (Figure S5). The graph suggests that the apparent R_S increases by between 0.2 nm and 8.2 nm per increase in FAE MV of 100 $Å^3$ (Figure S5). This correlation can be understood on the basis of the geometric correlations outlined above and the size-dependent ability of oils to partition into surfactant interfaces.[3,29,33,38,55,57] Specifically, we propose that an increase in FAE MV is associated with a decrease in FAE interfacial partition, which, in turn, increases the fraction of FAE located in the microemulsion droplets' core, decreases the A/V ratio and increases the apparent R_S of the aggregates. Indeed, these results and their proposed rationalisation are in good agreement with previous studies by *Eastoe et al.*, which report that the size of microemulsion droplets in PS-continuous PC lipid-stabilised systems increases with NPS chain length and attribute the correlation to a reduction in NPS interfacial penetration with NPS chain length.[55]

Interestingly, two of the PG/SPC/FAE systems, which comprise the smallest FAE studied, namely, methyl caprylate ($R_1R'_{8:0}$) or $R_2R'_{8:1,t2}$, predominantly produce microemulsions, which are

marginally smaller than the FAE-free micelles of equivalent SPC concentration (Figure 2 (A)). According to the geometric considerations above, these results support the proposed interfacial partition of FAE, as well as its dependence of FAE MV, and suggest that these two smallest FAE are predominantly localised in the SPC interface over a wide range of FAE concentrations.

Overall, the DLS results suggest that the aggregates in PG-rich PG/SPC/FAE mixtures are indeed microemulsion droplets and that their apparent R_S is governed by a combination of factors, namely the partition of PG and FAE into the SPC interface and the concentration of dispersed components (*i.e.*, SPC and FAE). Specifically, an increase in the concentration of components at the interface (*i.e.*, as a result of an increase in SPC concentration or solvent interfacial partition) was associated with an increase in the *A/V* ratio and decrease in the apparent R_S of the aggregates, while an increase in the component concentration in the microemulsion core (*i.e.*, due to decreasing FAE interfacial partition with increasing FAE concentration or MV) had the opposite effect. The morphology and localisation of the different components in the microemulsion droplets is examined next by SANS.

Morphology of the nanostructures by small-angle neutron scattering (SANS). A series of non-turbid PS-rich PG/SPC/FAE compositions were selected for SANS measurements. Since both the phase behaviour and DLS data suggest that the FAE structural feature that most strongly affects the self-assembly of the nonaqueous systems is MV, three FAE of low (330 Å^3), medium (440 Å^3) and high (593 Å^3) MV, *i.e.*, $R_2R'_{8:0}$, $R_2R'_{12:0}$ and $R_2R'_{18:1,c9}$, respectively, were employed in the study (Table 1).

Deuteration. To achieve scattering contrast, a combination of non-deuterated and deuterated components was used to prepare the samples. Specifically, the continuous phase was either non-deuterated PG or partially deuterated PG (1,2-propane-d$_6$-diol, d$_6$-PG) and the dispersed solvent

was either a non-deuterated FAE or a partially deuterated FAE (ethyl d_{15}-caprylate, d_{15}-$R_2R'_{8:0}$) at concentrations between 0 and 10% w/w. Additionally, since SPC is not commercially available in deuterated form, the PC lipid 1-palmitoyl-2-oleoyl-sn-glycero-3-phosphocholine (POPC, Figure S7), which is commercially available in partially deuterated form (*i.e.*, 1-palmitoyl-d_{31}-2-oleoyl-sn-glycero-3-phosphocholine, d_{31}-POPC), was used as the surfactant at a concentration of 5% w/w. The effect of this surfactant substitution is discussed in Supporting Material.

Deuterated lipid-stabilised systems have been reported to provide a reasonable structural analogue to equivalent non-deuterated systems under most conditions, except, notably, near phase boundaries.[76] Analogously, in this study, the phase behaviour of most samples remained unchanged upon deuteration (non-turbid), however, some compositions near a phase boundary (*i.e.*, mixtures of highest FAE concentration studied) became turbid. Hence, to characterise the selected compositions away from a phase boundary, the temperature for the SANS measurements was increased from RT and 25 °C (the temperatures used for phase behaviour and most DLS studies above, respectively) to 37 °C (a temperature relevant for pharmacological applications, at which the phase behaviour of samples of equivalent component concentrations but different deuteration was analogous). This increase in temperature is associated with a small increase in the microemulsion area in PG/SPC/FAE phase diagrams and a small decrease in the apparent R_S of FAE-in-PG microemulsion droplets, both of which are discussed further in Supporting Material.

Data fitting. Figure 3 shows the variation in neutron scattering intensity, *I(Q)*, as a function of scattering vector, *Q*, obtained for all (d_6-)PG/(d_{31}-)POPC(/FAE) compositions. Initial modelling of the data with a range of form factors for spheres, ellipsoids and cylinders with a core-shell structure suggested that the (d_{31}-)POPC head group, *i.e.*, PC, cannot be accounted for in any of the structures. This was attributed to the ability of PG to partition into surfactant interfaces and, thereby, reduce the scattering contrast, *Δρ*, between the phospholipid head groups and PS.

Molecular dynamics simulations of 1,2-dioleoyl-*sn*-glycero-3-phosphocholine[77] and 1,2-dipalmitoyl-*sn*-glycero-3-phosphocholine[78] (similar in structure to both POPC and SPC and comprising a PC group) have reported that as the concentration of PG in the bulk phase increases from 2.5 to 10 to 15 mol %, the total number of PG molecules coordinated to each phospholipid head group also increases from 0.7[78] to 1.8[77,78] to 2.2.[78] By extending this understanding to the nonaqueous mixtures in this study, we assume that at least 2.2 PG molecules per (d$_{31}$-)POPC lipid partition in the PC region. This, in turn, corresponds to a reduction in $\Delta\rho$ between the PC region and non-deuterated PS (PG) or deuterated PS (d$_6$-PG) from 1.75×10^{-6} Å^{-2} or 3.38×10^{-6} Å^{-2} to approx. 1×10^{-6} Å^{-2} or 2×10^{-6} Å^{-2}, respectively (individual SLD values are tabulated in Table S1). Since the PG concentration in all samples exceeds the highest PG concentration for which the total number of PG molecules coordinated to a PC group was reported,[77,78] it is conceivable that the number of coordinated PG molecules is higher than 2.2, thereby further reducing $\Delta\rho$. Based on these considerations, the surfactant head group region was assumed to be invisible in the analysis.

Next, the morphology of the remaining droplet components, namely the (d$_{31}$-)POPC tails group (1-palmitoyl-(d$_{31}$-)2-oleoyl, (d$_{31}$-)PO) and FAE, was considered. Initial analysis of the scattering curves suggested that the morphology of these components cannot be described using a core-shell dispersion model in which the (d$_{31}$-)PO and FAE regions are segregated into a shell and core, respectively; instead, acceptable fits could be obtained using particle dispersion models of uniform SLD. These initial fitting results support the proposed partition of FAE into the interfacial layer. Hence, a volume-weighted average of the SLD of the surfactant tails and FAE was used as the droplets SLD in the fitting of all scattering curves (Table S2).

Modelling using a range of dispersion morphologies (*e.g.*, spheres, prolate, oblate and triaxial ellipsoids and cylinders) showed that best fits are obtained using a triaxial ellipsoid model. This morphology has previously been observed in various mixed micellar systems,[79,80] including ones

stabilised by PC lipids in the presence of smaller amphiphiles.[81] The structure of triaxial ellipsoids can be described using three dimensions, *i.e.*, the minor (R_a), major (R_b) and polar (R_c) radii, which generally differ from each other.[82] Typically, R_a is comparable to the length of the amphiphile (ξ); R_b is determined by the spontaneous curvature of the interfacial layer (C_0) and increases from $\sim R_a$ (spherical cross-section cylinders) to $\sim R_c$ (discoidal structures) as C_0 decreases from ξ to $\frac{1}{4}\xi$ (or increases from $-\xi$ to $-\frac{1}{4}\xi$); and R_c is strongly dependent on the bending elastic constant, K, of the monolayer (as K increases R_c decreases).[82]
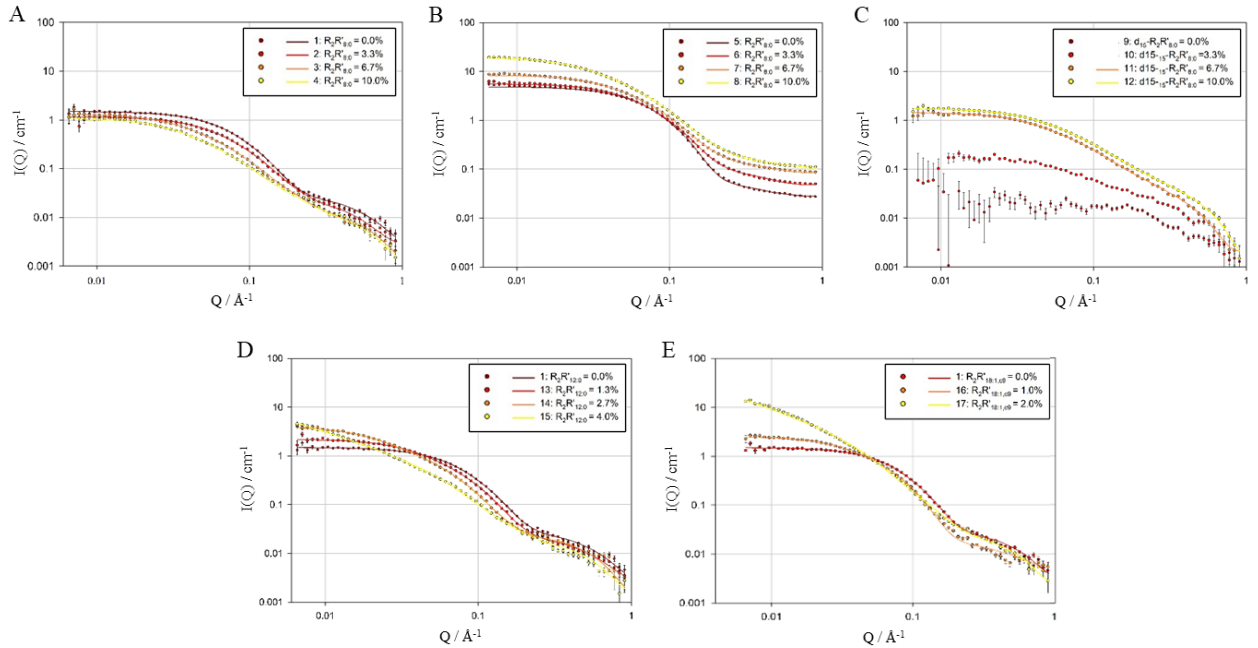

Figure 3. Scattering intensity curves obtained at 37 °C for: (A) PG/d$_{31}$-POPC/R$_2$R′$_{8:0}$; (B) d$_6$-PG/1-POPC/R$_2$R′$_{8:0}$; (C) PG/POPC/d$_{15}$-R$_2$R′$_{8:0}$; (D) PG/d$_{31}$-POPC/R$_2$R′$_{12:0}$; (E) PG/d$_{31}$-POPC/R$_2$R′$_{18:1,c9}$. Sample numbers and FAE concentration are shown in the legend. Filled circles represent experimental scattering data and lines - fits to the scattering curves. The composition and analysis results of all samples (sample number: 1-17) is detailed in Table 2.

Additionally, excess scattering was found at high Q values, which could not be accounted for by the triaxial ellipsoid model and suggested the presence of smaller dispersed objects. No evidence

of analogous structures was observed in the scattering curves of the pure solvents employed in the study. Given the substantially lower solvophobicity of phospholipids upon dispersion in nonaqueous PS when compared to water,[19] these additional structures were attributed to the presence of dispersed lipid molecules that exist alongside the larger ellipsoidal aggregates. Hence, in the SANS model-fitting performed here, these additional structures were modelled as spheres with SLD corresponding to the deuterated hydrocarbon chain of d_{31}-POPC (for d_{31}-POPC-stablised mixtures) or with the SLD of the POPC molecule (for POPC-stabilised mixtures).

In summary, all scattering curves were, therefore, fitted with the sum of a triaxial ellipsoid model and a spherical model, representing the morphology of the (d_{31}-)PO(/FAE) microemulsion droplet cores and (d_{31}-)POPC lipid molecules, respectively. As shown in Figure 3, excellent fits were obtained for all the mixtures studied (χ^2 values tabulated in Table S3).

General assessment of fitted morphologies. Before the fitting results are discussed in depth, the range of structural values obtained using the selected model-fitting is briefly assessed. To gauge whether the morphology obtained for the triaxial ellipsoids is reasonable, the range of R_a values was considered (Table 2). According to the model description in the previous subsection, the magnitude of R_a is expected to be comparable to the length of the surfactant, ξ (here, the length of the (d_{31}-)POPC tails, as the lipid head group area was not fitted).[82] While, to the best of our knowledge, no reports of the morphology of POPC aggregates in PG have been published to date, the self-assembly of POPC in aqueous solutions has been well-documented and the length of its tails group in planar and curved lamellar aggregates has been determined using SANS and neutron reflectivity to be between 13.2 ± 0.6 and 17.2 ± 0.7 Å.[83,84] Additionally, as discussed in the previous subsection, the solvents employed in this work, *i.e.*¸ PG and FAE, likely partition in the interfacial lipid layer to some extent. Studies have shown that the partition of small-to-medium amphiphiles in systems stabilised by PC lipids can considerably lower the average thickness of

mixed PC lipid/amphiphile monolayers and bilayers.[77,78,81] Indeed, the range of R_a values obtained for the triaxial ellipsoids (*i.e.*, between 5.6 Å and 16 Å, Table 2) is comparable or smaller than that previously reported for (d$_{31}$-)POPC tails group. Additionally, all triaxial ellipsoidal dimensions, *i.e.*, R_a, R_b, R_c, were found to vary considerably with FAE concentration (Table 2), which suggests FAE incorporation into the aggregates and supports the proposed structure for the samples, *i.e.*, that of microemulsions. The fitted morphology of the smaller dispersed objects is assessed in Supporting Material.

Location of solvents in the microemulsion droplets. The location of (d$_6$-)PG and FAE in the nanostructures is assessed next. For this purpose, the morphology of three sets of (d$_6$-)PG/ (d$_{31}$-)POPC/(d$_{15}$-)R$_2$R$'_{8:0}$ samples of varying isotropic contrast was examined (sample 1 – 12, Table 2; Figure 3 (A-C)). In particular, the three contrasts employed were a "shell" contrast, in which the deuterated component is d$_{31}$-POPC (sample 1-4, Table 2), a "drop" contrast, in which d$_6$-PG is used (sample 5-8, Table 2), and a "core" contrast, in which only the FAE is deuterated (sample 9-12, Table 2).

First, the location of (d$_6$-)PG with respect to (d$_{31}$-)POPC in the self-assembled triaxial ellipsoidal structures is considered. As described above, (d$_6$-)PG molecules were assumed to partition within the surfactant head group region to some extent, thereby effectively removing the contrast between the two. To assess the validity of this assumption, the nanostructure morphologies obtained from "shell" and "drop" contrast samples of equivalent R$_2$R$'_{8:0}$ concentration are compared (sample 1 - 8, Table 2). The former contrast variation provides information about the morphology of the d$_{31}$-PO surfactant tails and entrapped R$_2$R$'_{8:0}$, while the latter provides information about the morphology of the structures in which d$_6$-PG does not partition. If these two morphologies are equivalent, it would suggest that (d$_6$-)PG does not partition in the (d$_{31}$-)PO/R$_2$R$'_{8:0}$ aggregates but does mix with the (d$_{31}$-)POPC head groups to a significant extent, thereby making them invisible.

Indeed, a good agreement between the two sets of data is found (Table 2), with the average difference between compared pairs of droplet dimension (*e.g.,* R_a for sample 1 and R_a for sample 5) determined to be 0.2 ± 4.5 Å. This supports the assumption that (d_6-)PG can partition into the PC lipid head group area. The small differences between the "shell" and "drop" contrast morphologies appear to be largely non-directional (*i.e.*, neither of the two sets of aggregates is consistently larger or smaller than the other) and could be attributed to experimental errors, measurement uncertainties and/or the impact of the deuteration of different components in the sample sets.

Second, the location of the FAE, *i.e.*, (d_{15}-)$R_2R'_{8:0}$, in relation to the surfactant tails group, (d_{31}-)PO, is discussed. As described in the *Data fitting* subsection, preliminary analysis showed that the morphology of (d_{31}-)PO and FAE was best modelled with particle morphologies of uniform SLD, suggesting that the surfactant tails and FAE molecules are intermixed. To assess the validity of this proposition, the nanostructure morphologies obtained from "core" (isotropic contrast from d_{15}-$R_2R'_{8:0}$) and "shell" (isotropic contrast from d_{31}-PO) contrast samples of equivalent (d_{15}-)$R_2R'_{8:0}$ concentration are compared (sample 5 - 12, Table 2). An agreement between the morphologies of these two sample sets would suggest that (d_{31}-)PO and (d_{15}-)$R_2R'_{8:0}$ are fully intermixed within the microemulsion structures. At low d_{15}-$R_2R'_{8:0}$ concentration (0 or 3.3 % w/w), the scattering curves for "core" contrast samples could not be analysed due to the poor scattering contrast, $\Delta\rho$, between their components (sample 9 - 10, Figure 3 (C)). This lack of structural information was expected for sample 9 which comprises no deuterated components, however, it was not anticipated for sample 10 which contains 3.3 % w/w of d_{15}-$R_2R'_{8:0}$ (Table 2). To understand the unexpected results the scattering contrast in sample 10 was calculated assuming either full or no intermixing between the lipid tails and FAE. If no intermixing between the two components is present, a relatively large $\Delta\rho$ of 5.12×10^{-6} Å^{-2} between PO and d_{15}-$R_2R'_{8:0}$ would

be expected (Table S1). Conversely, if, as proposed above, the lipid tails and FAE intermix, then the resulting contrast between the mixed PO/FAE and the PC head group area would be significantly lower, *i.e.*, *ca.* 1.2×10^{-6} Å^{-2} (assuming that ~ 2.2 PG molecules per lipid partition into the PC area, see above), which indeed explains the poor scattering contrast in the data. This, therefore, supports the proposition that significant intermixing between d_{15}-$R_2R'_{8:0}$ and the lipid tails exists in the sample comprising 3.3 % w/w d_{15}-$R_2R'_{8:0}$. Similar reasoning has previously been employed in the literature to determine the extent of intermixing between components in triaxial ellipsoidal aggregates.[79] At higher d_{15}-$R_2R'_{8:0}$ concentration (6.7 or 10 % w/w), the scattering contrast between the microemulsion components was sufficient to allow the modelling of the "core" contrast samples and the resulting fitted morphologies were compared to those obtained for "shell" contrast samples of equivalent $R_2R'_{8:0}$ concentration (sample 7-8, 11-12, Table 2; Figure 3 (B, C)). The comparison shows that "core" contrast samples have smaller radii, *i.e.*, R_a, R_b and R_c, than the corresponding "shell" contrast samples (Table 2). These differences suggest that the concentration of $(d_{15}$-$)R_2R'_{8:0}$ molecules is comparably higher towards the centre of the microemulsion droplets than at their periphery, which, in turn, could be used as an indication for a decrease in solvent partition in the lipid interface and formation of microemulsion droplet cores comprising $(d_{15}$-$)R_2R'_{8:0}$ molecules. Nevertheless, as the differences in the dimensions of "core" and "shell" contrast sample are relatively small (~ 8.8 Å on average, Table 2), it is likely that some intermixing between the lipid and FAE molecules is still present in these structures. Interestingly, the magnitude of the differences between the fitted "core" and "shell" contrast morphologies increases as the $(d_{15}$-$)R_2R'_{8:0}$ concentration increases from 6.7 % w/w to 10 % w/w (Table 2), which suggests that the fraction of FAE molecules that partitions in the lipid interface decreases, while the fraction of FAE molecules that form the microemulsion core increases. Overall, the comparison of the "core" and "shell" contrast data suggests that as the concentration of $(d_{15}$-$)R_2R'_{8:0}$ increases

from 3.3 to 10 % w/w, the fraction of $(d_{15}-)R_2R'_{8:0}$ molecules that partition into the $(d_{31}-)POPC$ interface decreases and the formation of microemulsion cores, which are slightly smaller than the $d_{31}-PO/R_2R'_{8:0}$ structures, is observed. These observations agree well with the discussion of DLS results above, where an increase in FAE concentration was speculated to decrease the fraction of FAE molecules that partition in the interfacial monolayer, thereby promoting the formation of FAE cores comprising the non-partitioning FAE.

Effect of FAE concentration and MV. Lastly, to understand the effects of FAE concentration and MV on the morphology of the nonaqueous microemulsion droplets, the series of "shell" contrast $PG/d_{31}-POPC/FAE$ samples, which comprise different concentrations of $R_2R'_{8:0}$, $R_2R'_{12:0}$ or $R_2R'_{18:1,c9}$ as the FAE, are considered (sample 1-4, 13-17, Table 2; Figure 3 (A, D, E)).

To facilitate the discussion, the typical effects of amphiphile addition on the interfacial properties, which influence the morphology of triaxial ellipsoidal micelles, *i.e.*, the thickness, spontaneous curvature (C_0) and bending elastic constant (K) of the surfactant monolayer (see *Data fitting* subsections),[82] is discussed first. As mentioned above, previous studies have shown that the incorporation of small-to-medium amphiphiles in systems stabilised by PC lipids can considerably lower the thickness of mixed PC lipid/amphiphile monolayers and bilayers.[77,78,81] Additionally, C_0 has been suggested to increase upon the addition of short chain amphiphiles to monolayers stabilised by longer chain surfactants,[68] whereas the value of K is generally brought down by the process of mixing two amphiphiles.[68,85] Therefore, we hypothesise that an increase in FAE interfacial partition in the FAE-in-PG $(d_{31}-)POPC$-stabilised microemulsions would generally decrease the interfacial thickness and K and increase C_0, thereby resulting in a decrease in R_a and R_b and increase in R_c of the aggregates.[82]

Table 2. Morphology of triaxial ellipsoidal aggregates in (d$_6$-)PG/(d$_{31}$-)POPC(/FAE) samples of described composition obtained using small-angle neutron scattering (SANS) at 37 °C. ([a] Values outside of dimensions covered by the Q-range and hence only indicative of the significant droplet elongation).

Propylene glycol / d$_{31}$-POPC / ethyl caprylate (Shell contrast)			
PS/S/FAE (% w/w)	95/5/0 (Sample 3.1)	91.7/5/3.3 (Sample 3.2)	88.3/5/6.7 (Sample 3.3)	85/5/10 (Sample 4)
**R$_a$	R$_b$	R$_c$ (Å)**	13.3	22.8	47.6	11.6	23.1	54.9	9.3	28.2	83.1	6.2	29.5	97.6

1,2-Propane-d$_6$-diol / POPC / ethyl caprylate (Drop contrast)			
PS/S/FAE (% w/w)	95/5/0 (Sample 3.5)	91.7/5/3.3 (Sample 3.6)	88.3/5/6.7 (Sample 3.7)	85/5/10 (Sample 3.8)
**R$_a$	R$_b$	R$_c$ (Å)**	14.3	23.2	48.0	12.6	23.6	56.6	11.6	25.1	71.0	10.3	29.4	103.8

Propylene glycol / POPC / ethyl d$_{15}$-caprylate (Core contrast)			
PS/S/FAE (% w/w)	95/5/0 (Sample 3.9)	91.7/5/3.3 (Sample 3.10)	88.3/5/6.7 (Sample 3.11)	85/5/10 (Sample 3.12)
**R$_a$	R$_b$	R$_c$ (Å)**	-	-	6.0	22.7	74.8	5.6	21.9	70.4
	-	-		

Propylene glycol / d$_{31}$-POPC / ethyl laurate (Shell contrast)		
PS/S/FAE (% w/w)	93.7/5/1.3 (Sample 3.13)	92.3/5/2.7 (Sample 3.14)	91/5/4 (Sample 3.15)
**R$_a$	R$_b$	R$_c$ (Å)**	13.7	25.5	78.8	15.0	33.0	151.4	6.3	39.6	1714.1 [a]
			x 25

Propylene glycol / d$_{31}$-POPC / ethyl oleate (Shell contrast)	
PS/S/FAE (% w/w)	94/5/1 (Sample 3.16)	93/5/2 (Sample 3.17)
**R$_a$	R$_b$	R$_c$ (Å)**	16.0	26.2	85.8	11.2	53.3	1350.2 [a]
		x 10

Legend		
Polar solvent (PS)	**Surfactant (S)**	**Fatty acid ester (FAE)**
Propylene glycol (PG)	1-palmitoyl-2-oleoyl-sn-glycero-3-phosphocholine (POPC)	Ethyl caprylate (R$_2$R`$_{8:0}$)	Ethyl laurate (R$_2$R`$_{12:0}$)
1,2-Propane-d$_6$-diol (d$_6$-PG)	1-palmitoyl-d31-2-oleoyl-sn-glycero-3-phosphocholine (d$_{31}$-POPC)	Ethyl d$_{15}$-caprylate (d$_{15}$-R$_2$R`$_{8:0}$)	Ethyl oleate (R$_2$R`$_{18:1,c9}$)

Based on the outlined hypotheses, the variations in droplet dimensions with FAE MV are assessed first. As shown in Table 2, all triaxial ellipsoidal radii, *i.e.*, R_a, R_b and R_c, increase with increasing FAE MV. According to the considerations above, both the changes in R_a and R_b can be attributed to a reduced FAE interfacial partition with increasing FAE MV - a correlation that was also discussed in the phase behaviour and DLS studies. This association also agrees with previous reports of the size-dependent partition of NPS in the surfactant interface of other microemulsifying systems.[3,29,33,38,55,57] Nonetheless, the increase in R_c with FAE MV cannot be ascribed to the proposed FAE interfacial partition decrease, which, according to the hypotheses above, would promote a decrease in R_c. Instead, these results could be examined in the context of the negative correlation that has been observed between the monolayer rigidity (expressed as K or $2K + \overline{K}$, where $\overline{K}$ is the Gaussian elastic modulus) of microemulsifying systems stabilised by PC lipids[55] or Aerosol-OT[29,49,69] and NPS MV (*cf.* Introduction). We propose that an analogous decrease in K with an increase in FAE MV would explain the increase in R_c (due to the negative correlation between R_c and K, Table 2).[82] This proposition is in agreement not only with our SANS data and the studies cited above, but also the above phase behaviour studies and the Langmuir trough monolayer experiments that follow.

Next, the effect of FAE concentration on the triaxial ellipsoidal radii is briefly discussed. The results suggest that for each of the PG/d$_{31}$-POPC/FAE sets of samples, an increase in FAE concentration is generally associated with a decrease in R_a and an increase in both R_b and R_c (Table 2). First, as outlined in the hypotheses above, both the decrease in R_a and increase in R_c are indicative of an increase in the amount of FAE molecules that partition in the d$_{31}$-POPC monolayer. The increase in the net number of FAE molecules at the microemulsion droplets interface with an increase in FAE concentration is expected. Nevertheless, the changes of R_b appears not to be guided by the proposed increase in FAE molecules at the PG/FAE interface, which according to

the outlined hypothesis would decrease R_b. Instead, the changes observed can be speculatively attributed to the proposition that an increase in FAE concentration is associated with a decrease in the fraction of FAE molecules that partition into the surfactant interface and the formation of a microemulsion core comprising an increasing fraction of FAE molecules that do not partition in the interface. Based on the geometrical considerations and experimental observations in the DLS results section, an increase in FAE concentration is, hence, expected to increase both the fraction and net amount of FAE molecules located in the microemulsion core, thereby swelling the microemulsion droplets. We propose that this increase in microemulsion core size with FAE concentration is responsible for the observed increase in R_b and, perhaps, to some extent, for the increase in R_c. Overall, as the FAE concentration increases, both the overall number of FAE molecules that partition into the interfacial monolayer increases (as suggested by the changes in R_a and R_c) and the overall number of FAE molecules that form the microemulsion core increases (as suggested by the contrast variation studies and the changes in R_b (and R_c) here), while the fraction of the interfacial to microemulsion core FAE decreases (as supported by the DLS results above).

In summary, the SANS data modelling suggests that the morphology of the PS-rich (d_6-)PG/(d_{31}-)POPC(/FAE) aggregates can be reasonably fitted using a triaxial ellipsoid model. The results thus support the formation of microemulsion droplets, and the partition of some (d_6-)PG molecules in the PC head group area. The intermixing between the FAE and (d_{31}-)POPC monolayer was hypothesised to decrease with increase in both FAE MV and concentration. An elongation of the triaxial ellipsoidal structures was recorded with increasing FAE MV and was hypothesised to arise from a decrease in monolayer rigidity. This speculation is studied in more detail in the following section, where changes in monolayer elastic properties with composition are elucidated.

Interfacial behaviour with Langmuir trough (LT) monolayer studies. The results of the phase behaviour, DLS and SANS studies above all suggest that the FAE employed in this work partition within the interfacial layer of SPC- and POPC-stabilised microemulsions to some extent. Therefore, to gain further insight into the effect of the eleven FAE (Table 1) on the properties of the SPC-stabilised systems, it is important to understand the interactions between SPC and FAE at the interface between hydrophilic and hydrophobic environments. To this end, the behaviour of SPC in the presence of equimolar amounts of one or a combination of FAE was studied at room temperature (RT, 23 ± 2 °C) using LT monolayer compression experiments. The polar solvent used in these experiments was purified water instead of PG due to technical difficulties related to the use of PG as a subphase, *i.e.*, increased solubility of SPC[19] and some FAE[67] in PG and hygroscopicity of PG,[35] which result in the formation of constantly evolving systems. As suggested in the discussion of the phase behaviour and DLS results above, the substitution of PG with water is expected to considerably affect the interfacial properties of SPC monolayers. Nonetheless, these studies still bring valuable information of the influence of FAE molecular structures on the interfacial behaviour of SPC.

Interfacial behaviour of individual components. Before the interactions between SPC and FAE at the air/water interface are discussed, the interfacial behaviour of the individual components is briefly considered. First, the limiting area per SPC molecule at the air/water interface obtained here is 86 ± 3 Å^2/molecule (Table 3), which agrees well with previously reported limiting area values for the lipid of $78 - 103$ Å^2/ molecule.[65,86] Second, although the isotherms of the individual FAE were not experimentally determined here, LT data for fatty acids (FA), fatty alcohols (FAlc) fatty amines (FAm) and FAE of similar structure, MV, water solubility and hydrophobicity have previously been reported in the literature. In particular, saturated fatty acid derivatives have been reported to have a limiting area that is largely independent of fatty acid chain length and ranging

between approx. 19 and 26 Å^2/molecule,[64,66,86,87] while unsaturated and bulkier fatty acid derivatives can have a significantly increases limiting areas.[66,87]
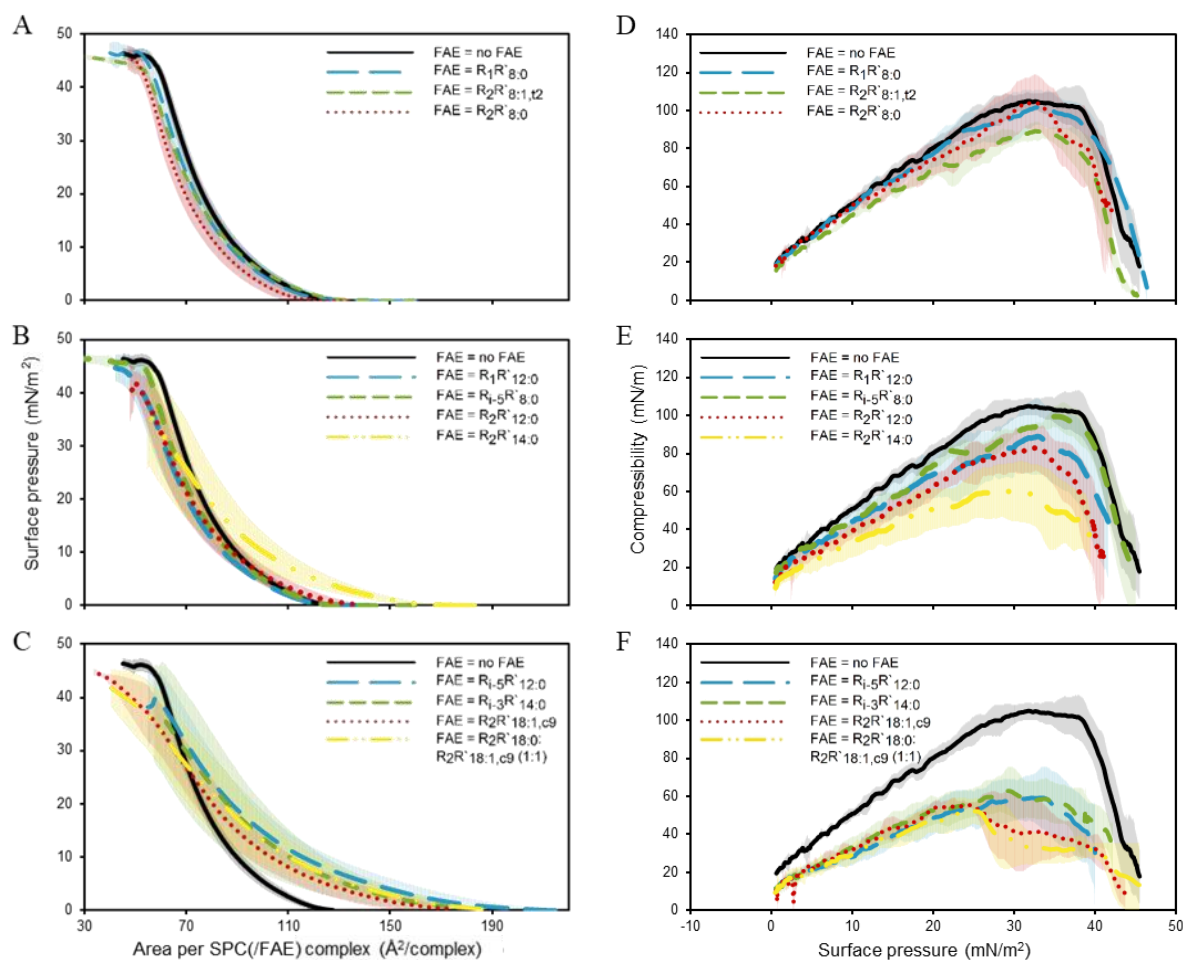

Figure 4. Average surface pressure-area per complex (π-A_c) isotherms (A-C) and compressibility curves (D-F) for SPC(/FAE) monolayers obtained in a Langmuir trough at 23 ± 2 °C (n = 4-7). The standard deviation for the measurements is shown as a shadow behind the curves. The following FAE were employed in order of increasing molecular volume: (A/D) methyl caprylate (R$_1$R'$_{8:0}$, — —), ethyl octenoate (R$_2$R'$_{8:1,t2}$, - -), ethyl caprylate (R$_2$R'$_{8:0}$, • •); (B/E) methyl laurate (R$_1$R'$_{12:0}$, — —), isoamyl caprylate (R$_{i-5}$R'$_{8:0}$, - -), ethyl laurate (R$_2$R'$_{12:0}$, • •); ethyl myristate (R$_2$R'$_{14:0}$, — • •); (C/F) isoamyl laurate (R$_{i-5}$R'$_{12:0}$, — —), isopropyl myristate (R$_{i-3}$R'$_{14:0}$, - -), ethyl oleate (R$_2$R'$_{18:1,c9}$, • •), ethyl stearate:ethyl oleate (1:1) (R$_2$R'$_{18:0}$:R$_2$R'$_{18:1,c9}$ (1:1), — • •).

Interfacial behaviour of mixed SPC/FAE monolayers. Figure 4 shows the surface pressure-area per complex, π-A_c, isotherms and compressibility curves for all 12 SPC(/FAE) systems of composition detailed in Table 3. To facilitate the analysis of the data, two assumptions were made. First, SPC and FAE molecules at the air/water interface were assumed to be homogeneously mixed. Indeed, as can be seen in Figure 4 (A-C), all π-A_c isotherms exhibit a single collapse pressure, π_{coll}, which, in agreement with literature,[66] can be used to support this proposition. Second, based on previous LT studies of the interfacial behaviour of mixtures of PC lipids and amphiphiles (*i.e.*, FA, FAlc or FAm) that suggest the formation of stable 1:1 PC/amphiphile complexes,[64,86] the systems here are also treated as 1:1 SPC/FAE complexes.

The influence of FAE addition and structure (molecular volume, R′ group saturation and R group branching, Table 1) on the interfacial properties of the SPC(/FAE) monolayers (Figure 4, Table 3) is examined next. It should be noted that changes in FAE branching and saturation were not associated with significant changes in the interfacial properties of the systems (Table 3). These observations could be largely attributed to the small number of branched or unsaturated FAE studied here and agree well with the limited effect of these FAE properties on the phase behaviour of PG/SPC/FAE systems and on the FAE-in-PG microemulsion droplets size discussed in previous sections. To assess the effect of the remaining composition variables, *i.e.*, FAE presence and MV, on the behaviour of the SPC(/FAE) mixtures at the air/water interface, the π-A_c isotherms and compressibility curves for the monolayers were compared (Figure 4). The differences in short- and long-range molecular interactions between the twelve systems were elucidated using the limiting surface areas and lift-off areas, respectively, while the changes in monolayer elastic properties were determined using maximum compressibility moduli, $C_s^{-1}{}_{max}$ (Table 3).

First, the influence of FAE presence and MV on the short-range interactions in SPC monolayers is examined. For this purpose, the limiting surface area of each SPC/FAE complex, $A_{c,lim}$, *i.e.*, the

area occupied by the complex in the gaseous state (*i.e.*, at $\pi = 0$ mN/m^2, Table 3), was compared to the sum of the limiting areas of its components. The comparisons suggest that the $A_{c,lim}$ values for SPC/FAE complexes (between 80 ± 3 and 110 ± 5 Å^2/molecule, Table 3) are typically smaller than the sum of the limiting areas of their components, *i.e.*, SPC (86 ± 3 Å^2/molecule) and FAE (at least ~ 20 Å^2/molecule[64,66,86,87]). In agreement with the literature,[66,86] we propose that these observations can be attributed to attractive interactions between SPC and FAE molecules and shielding of the electrostatic repulsions between zwitterionic PC head groups by FAE molecules, both of which contribute to a reduction in the area occupied by each amphiphile in the mixed monolayers. Additionally, the data suggests that the magnitude of this reduction gradually decreases with increase in FAE MV (Table 3). We speculate that these differences can be attributed to an increase in the space taken up by larger amphiphiles in the mixed monolayer and subsequent changes in monolayer packing and molecular orientation at the air/water interface.

Second, the FAE's influence on the long-range interfacial interactions is discussed. For this purpose, a comparison between the twelve SPC(/FAE) lift-off areas (*i.e.*, the A_c values at which π starts to increase, thereby indicating the onset of interactions between the molecules at the air/water interface) was drawn (Table 3). The comparison suggests that upon addition of FAE to the SPC monolayer, the lift-off area typically increases (Table 3, Figure 4 (A-C)). In agreement with the literature[87,89] and above discussion of short-range interactions in SPC(/FAE) monolayers, these changes can be speculatively attributed to an increase in the attractive forces between SPC and FAE molecules and, hence, an increase in the longest interfacial distance at which these amphiphiles interact. Additionally, upon an increase in FAE MV, an increase in the lift-off area per SPC/FAE complex is generally observed (Table 3), which suggests that the long-range intermolecular attractive forces between larger FAE and SPC are stronger than those between smaller FAE and SPC.

Table 3. Average composition, lift-off and limiting areas per complex and maximum compressibility obtained for SPC/FAE systems at the air/water interface at 23 ± 2 °C (n = 4-7). FAE in order of increasing molecular volume: methyl caprylate ($R_1R'_{8:0}$), ethyl octenoate ($R_2R'_{8:1,t2}$), ethyl caprylate ($R_2R'_{8:0}$), methyl laurate ($R_1R'_{12:0}$), isoamyl caprylate ($R_{i\text{-}5}R'_{8:0}$), ethyl laurate ($R_2R'_{12:0}$), ethyl myristate ($R_2R'_{14:0}$), isoamyl laurate ($R_{i\text{-}5}R'_{12:0}$), isopropyl myristate ($R_{i\text{-}3}R'_{14:0}$), ethyl oleate ($R_2R'_{18:1,c9}$), ethyl stearate:ethyl oleate (1:1) ($R_2R'_{18:0}$:$R_2R'_{18:1,c9}$ (1:1)). The statistical significances of the differences in the areas and compressibility of SPC/FAE monolayers when compared to the SPC monolayer are shown ($p < 0.05$ (*), $p < 0.001$ (***)).

Components (SPC/FAE)	Composition (SPC:FAE (:FAE)) (mol ratio)	Limiting area, $A_{c,lim}$ (Å^2/complex)	Lift-off area (Å^2/complex)	Maximum compressibility, $C_s^{-1}{}_{max}$ (mN/m)
SPC/-	-	86 ± 3	121 ± 3	105 ± 4
SPC/$R_1R'_{8:0}$	1:1	84 ± 5	122 ± 8	102 ± 9
SPC/$R_2R'_{8:1,t2}$	1:1	84 ± 3	128 ± 1	89 ± 5
SPC/$R_2R'_{8:0}$	1:1	80 ± 3	116 ± 6	104 ± 13
SPC/$R_1R'_{12:0}$	1:1	83 ± 2	125 ± 5	89 ± 20
SPC/$R_{i\text{-}5}R'_{8:0}$	1:1	83 ± 2	126 ± 3	100 ± 5
SPC/$R_2R'_{12:0}$	1:1	84 ± 4	134 ± 8	$83 \pm 12^{*}$
SPC/$R_2R'_{14:0}$	1:1	97 ± 16	$161 \pm 8^{***}$	$61 \pm 14^{***}$
SPC/$R_{i\text{-}5}R'_{12:0}$	1:1	107 ± 15	$186 \pm 16^{***}$	$59 \pm 16^{***}$
SPC/$R_{i\text{-}3}R'_{14:0}$	1:1	103 ± 20	$176 \pm 18^{***}$	$63 \pm 13^{***}$
SPC/$R_2R'_{18:1,c9}$	1:1	103 ± 8	$166 \pm 11^{***}$	$56 \pm 1^{***}$
SPC/$R_2R'_{18:1,c9}$/$R_2R'_{18:0}$	1:0.5:0.5	$110 \pm 15^{*}$	$197 \pm 10^{***}$	$52 \pm 7^{***}$

Lastly, the influence of FAE presence and MV on the elastic properties of the mixed monolayers is elucidated using the maximum area compressibility moduli, $C_s^{-1}{}_{max}$, of the SPC/FAE mixtures tabulated in Table 3. The results suggest that the incorporation of FAE and increase in FAE MV are both correlated with a decrease $C_s^{-1}{}_{max}$ (Table 3). Based on the mechanical properties of polymer brushes, the relationship between the area compressibility modulus, C_s^{-1}, and the bending elastic modulus, K, of PC lipid monolayers at a given π has been shown to be well described by: $C_s^{-1} = 24 \times \frac{K}{t_t^2}$, where t_t is thickness of the lipid hydrocarbon tail group area.[71] Hence, the observed decrease in $C_s^{-1}{}_{max}$ with FAE incorporation and MV can be qualitatively associated with

a decrease in K for the corresponding SPC/FAE monolayers, in agreement with the proposition made in the SANS and phase behaviour studies.

Overall, the Langmuir trough monolayer studies suggest that the addition of equimolar amounts of FAE to SPC monolayers and the increase in FAE MV both result in an increase in the attractive interactions between the amphiphiles at the air/water interface. Additionally, the incorporation of FAE and increase in FAE MV were also associated with a decrease in the maximum area compressibility moduli of the monolayers, which, in turn, is associated with a decrease in the monolayer bending elastic moduli, K.

Conclusion

The phase behaviour, morphology and interfacial properties of nonaqueous mixtures of pharmaceutically acceptable components, *i.e.*, soybean phosphatidylcholine (SPC) as the surfactant, propylene glycol (PG) as the polar solvent (PS) and fatty acid esters (FAE) as the non-polar solvent, were studied with the aim of determining the influence of FAE molecular structure on the existence and characteristics of microemulsions in the systems.

Microemulsification in the PG/SPC/FAE systems was facilitated by the substitution of water with PG. Compared to analogous aqueous SPC-stabilised systems, the nonaqueous systems formed significantly larger microemulsion areas of existence and required less surfactant to microemulsify. Additionally, FAE-in-PG microemulsion droplets were determined to be comparable or smaller than those formed in similar aqueous systems. These differences in aggregation behaviour were attributed to the ability of PG to partition into the SPC interfacial layer and alter its properties as confirmed by small-angle neutron scattering (SANS) measurements on analogous PG/1-palmitoyl-2-oleoyl-*sn*-glycero-3-phosphocholine(POPC)/FAE systems.

To determine the effect of FAE molecular structure on the formation and properties of PG/SPC/FAE microemulsions, eleven FAE of varying molecular volume (MV), alcohol group (R) branching and fatty acid group (R′) saturation were employed (Table 1). The influence of FAE MV on the system's properties was most notable, while R branching and R′ saturation both had a smaller (or insignificant) impact on the bulk and interfacial behaviour of the mixtures.

The phase behaviour studies suggested that an increase in FAE MV from 299 Å^3 to 409 Å^3 is correlated with a significant decrease in the microemulsion phase diagram area (particularly in the region of FAE-in-PG microemulsion formation). This was attributed to a decrease in FAE partition into the interfacial SPC layer, which, in turn, is associated with a decrease in spontaneous interfacial curvature, C_0, and, hence, in the range of compositions that form microemulsions of

positive C_0, such as FAE-in-PG microemulsions. Further increase in FAE MV (up to 611 Å^3) was not associated with notable changes in phase behaviour. This was attributed to a decrease in the bending elastic modulus, K, of the lipid monolayer, which, in turn favours the formation of microemulsions over an increased range of principal interfacial curvatures and counterbalances the effect of the changes in FAE interfacial partition. DLS data suggest that an increase in FAE MV and concentration is associated with an increase in the apparent radius of solvation (R_S) of the aggregates that was attributed to a decrease in FAE interfacial partition and consequent microemulsion core formation and swelling. SANS data of FAE-in-PG POPC-stabilised microemulsions were fitted by a triaxial ellipsoid model, in which both the PS and NPS partition to a significant extent. A decrease in the minor ellipsoidal radius with a decrease in FAE MV and increase in FAE concentration was attributed to an increased FAE interfacial partition, while an increase in the polar radii of the aggregates with FAE MV and concentration was attributed to a decrease in the bending elastic moduli of the interfacial monolayer. Finally, LT monolayer studies suggest that an increase in FAE MV is associated with a decrease in the maximum area compressibility moduli of equimolar SPC/FAE mixed monolayers at the air/water interface, which, in turn, is associated with a decrease in K and supports the proposed correlations in the phase behaviour and SANS data.

The detailed structural investigation presented here provides evidence that the use of the lipid SPC in nonaqueous systems containing PG as polar solvent and FAE as non-polar solvent allows the preparation of low surfactant concentration, FAE-in-PG microemulsions that are potentially suitable for use in the pharmaceutical, cosmetic and food formulations. Moreover, the study offers an in-depth understanding of the relationship between FAE molecular structure and microemulsion formation, morphology and monolayer elastic properties, allowing the selection of FAE suitable for various applications.

Acknowledgment

References

(1)   Hoar, T. P.; Schulman, J. H. Transparent water-in-oil dispersions: The oleopathic hydro-micelle [1]. *Nature* **1943**, *152*, 102-103.

(2)   Schulman, J. H.; Stoeckenius, W.; Prince, L. M. Mechanism of formation and structure of micro emulsions by electron microscopy. *Journal of Physical Chemistry* **1959**, *63*, 1677-1680.

(3)   Langevin, D. Micelles and microemulsions. *Annual Review of Physical Chemistry* **1992**, *43*, 341-369.

(4)   Paul, B.; Moulik, S. The Viscosity Behaviours of Microemulsions: An Overview. *Proceedings of the Indian National Science Academy* **2000**, *66*, 499-519.

(5)   Lawrence, M. J.; Rees, G. D. Microemulsion-based media as novel drug delivery systems. *Advanced Drug Delivery Reviews* **2000**, *45*, 89-121.

(6)   Radi, M.; Abbasi, S. Optimization of Novel Oil Extraction Technique From Canola Seeds: Lecithin-Based Microemulsion. *European Journal of Lipid Science and Technology* **2018**, *120*.

(7)   Buckley, P.; Hargreaves, N.; Cooper, S. Nucleation of quartz under ambient conditions. *Communications Chemistry* **2018**, *1*, 1-10.

(8)   Subinya, M.; Steudle, A. K.; Nestl, B.; Nebel, B.; Hauer, B.; Stubenrauch, C.; Engelskirchen, S. Physicochemical aspects of lipase B from *candida antarctica* in bicontinuous microemulsions. *Langmuir* **2014**, *30*, 2993-3000.

(9)   Novartis. Cyclosporin - Allergan: Ciclosporin - Allergan, cyclosporin ophthalmic emulsion, cyclosporin - Allergan, Restasis™. *Drugs in R and D* **2003**, *4*, 126-127.

(10)   Zhang, L.; Sun, X.; Xiang, D.; Zhang, Z. R. Formulation and physicochemical characterization of norcantharidin microemulsion containing lecithin-based surfactants. *Journal of Drug Delivery Science and Technology* **2004**, *14*, 461-469.

(11)   Moreno, M. A.; Ballesteros, M. P.; Frutos, P. Lecithin-based oil-in-water microemulsions for parenteral use: Pseudoternary phase diagrams, characterization and toxicity studies. *Journal of Pharmaceutical Sciences* **2003**, *92*, 1428-1437.

(12)   Aboofazeli, R.; Lawrence, M. J. Investigations into the formation and characterization of phospholipid microemulsions. I. Pseudo-ternary phase diagrams of systems containing water-lecithin-alcohol-isopropyl myristate. *International Journal of Pharmaceutics* **1993**, *93*, 161-175.

(13)   Aboofazeli, R.; Lawrence, C. B.; Wicks, S. R.; Lawrence, M. J. Investigations into the formation and characterization of phospholipid microemulsions. III. Pseudo-ternary phase diagrams of systems containing water-lecithin-isopropyl myristate and either an alkanoic acid, amine, alkanediol, polyethylene glycol alkyl ether or alcohol as cosurfactant. *International Journal of Pharmaceutics* **1994**, *111*, 63-72.

(14)   Saint Ruth, H.; Attwood, D.; Ktistis, G.; Taylor, C. J. Phase studies and particle size analysis of oil-in-water phospholipid microemulsions. *International Journal of Pharmaceutics* **1995**, *116*, 253-261.

(15)   Leonardi, A.; Bucolo, C.; Romano, G. L.; Platania, C. B. M.; Drago, F.; Puglisi, G.; Pignatello, R. Influence of different surfactants on the technological properties and in vivo ocular tolerability of lipid nanoparticles. *International Journal of Pharmaceutics* **2014**, *470*, 133-140.

(16)   Direct food substances affirmed as generally recognized as safe. In *21*; Food and Drug Administration, D. o. H. a. H. S., Ed.: Code of Federal Regulations, 2019.

(17)   List, G. R.: 1 - Soybean Lecithin: Food, Industrial Uses, and Other Applications. In *Polar Lipids*; Ahmad, M. U., Xu, X., Eds.; Elsevier, 2015; pp 1-33.

(18)   Parnham, M. J.: Safety and tolerability of intraveneously administered phopspholipids and emulsions. In *Emulsions and Nanosuspensions for the Formulation of Poorly Soluble Drugs*; Muller, R. H., Benita, S., B., B., Eds.; Medpharm Scientific Publishers: Stuttgart, 1998; Vol. 212; pp 131-142.

(19)   Shchipunov, A. Y. Self-organising structures of lecithin. *Russian Chemical Reviews* **1997**, *66*, 301-322.

(20)   Israelachvili, J. N.; Mitchell, D. J.; Ninham, B. W. Theory of self-assembly of hydrocarbon amphiphiles into micelles and bilayers. *Journal of the Chemical Society, Faraday Transactions 2: Molecular and Chemical Physics* **1976**, *72*, 1525-1568.

(21)   Angelico, R.; Ceglie, A.; Colafemmina, G.; Delfine, F.; Olsson, U.; Palazzo, G. Phase behavior of the lecithin/water/isooctane and lecithin/water/decane systems. *Langmuir* **2004**, *20*, 619-631.

(22)   Shinoda, K.; Araki, M.; Sadaghiani, A.; Khan, A.; Lindman, B. Lecithin-based microemulsions: Phase behavior and microstructure. *Journal of Physical Chemistry* **1991**, *95*, 989-993.

(23)   Israelachvili, J. The science and applications of emulsions — an overview. *Colloids and Surfaces A: Physicochemical and Engineering Aspects* **1994**, *91*, 1-8.

(24)   Eastoe, J.: Microemulsions. In *Surfactant Chemistry*; Cosgrove, T., Ed.; Wuhan University Press, 2005; pp 77-97.

(25)   Von Corswant, C.; Söderman, O. Effect of adding isopropyl myristate to microemulsions based on soybean phosphatidylcholine and triglycerides. *Langmuir* **1998**, *14*, 3506-3511.

(26)   Beblik, G.; Servuss, R. M.; Helfrich, W. Bilayer bending rigidity of some synthetic lecithins. *J. Phys. France* **1985**, *46*, 1773-1778.

(27)   De Gennes, P. G.; Taupin, C. Microemulsions and the flexibility of oil/water interfaces. *Journal of Physical Chemistry* **1982**, *86*, 2294-2304.

(28)   Angelico, R.; Ceglie, A.; Olsson, U.; Palazzo, G. Phase diagram and phase properties of the system lecithin-water-cyclohexane. *Langmuir* **2000**, *16*, 2124-2132.

(29)   Kellay, H.; Binks, B. P.; Hendrikx, Y.; Lee, L. T.; Meunier, J. Properties of surfactant monolayers in relation to microemulsion phase behaviour. *Advances in Colloid and Interface Science* **1994**, *49*, 85-112.

(30)   Nguyen, T. T. L.; Edelen, A.; Neighbors, B.; Sabatini, D. A. Biocompatible lecithin-based microemulsions with rhamnolipid and sophorolipid biosurfactants: Formulation and potential applications. *Journal of Colloid and Interface Science* **2010**, *348*, 498-504.

(31)   Kotmakchiev, M.; Kantarci, G.; Çetintaş, V. B.; Ertan, G. Cytotoxicity of a novel oil/water microemulsion system loaded with mitomycin-C in in vitro lung cancer models. *Drug Development Research* **2012**, *73*, 185-195.

(32)   Friberg, E.; Podzimek, M. A non-aqueous microemulsion. *Colloid & Polymer Science* **1984**, *262*, 252-253.

(33)   Patel, N.; Schmid, U.; Lawrence, M. J. Phospholipid-based microemulsions suitable for use in foods. *Journal of Agricultural and Food Chemistry* **2006**, *54*, 7817-7824.

(34)   Hill, R. M.; Lawrence, M. J.: Microemulsions: Dielectric Spectroscopy. In *Encyclopedia of Surface and Colloid Science*; Somasundaran, P., Ed.; CRC Press, 2002.

(35)   Sullivan, C. J.; Kuenz, A.; Vorlop, K. D.: Propanediols. In *Ullmann's Encyclopedia of Industrial Chemistry*, 2018; pp 233-241.

(36)   Yotsawimonwat, S.; Okonoki, S.; Krauel, K.; Sirithunyalug, J.; Sirithunyalug, B.; Rades, T. Characterisation of microemulsions containing orange oil with water and propylene glycol as hydrophilic components. *Die Pharmazie* **2006**, *61*, 920-926.

(37)   Garti, N.; Yaghmur, A.; Leser, M. E.; Clement, V.; Watzke, H. J. Improved Oil Solubilization in Oil/Water Food Grade Microemulsions in the Presence of Polyols and Ethanol. *Journal of Agricultural and Food Chemistry* **2001**, *49*, 2552-2562.

(38)   Yaghmur, A.; Aserin, A.; Garti, N. Phase behavior of microemulsions based on food-grade nonionic surfactants: Effect of polyols and short-chain alcohols. *Colloids and Surfaces A: Physicochemical and Engineering Aspects* **2002**, *209*, 71-81.

(39)   Yaghmur, A.; Aserin, A.; Antalek, B.; Garti, N. Microstructure considerations of new five-component Winsor IV food-grade microemulsions studied by pulsed gradient spin-echo NMR, conductivity, and viscosity. *Langmuir* **2003**, *19*, 1063-1068.

(40)   Yaghmur, A.; de Campo, L.; Aserin, A.; Garti, N.; Glatter, O. Structural characterization of five-component food grade oil-in-water nonionic microemulsions. *Physical Chemistry Chemical Physics* **2004**, *6*, 1524-1533.

(41)   Kim, S.; Ng, W. K.; Shen, S.; Dong, Y.; Tan, R. B. H. Phase behavior, microstructure transition, and antiradical activity of sucrose laurate/propylene glycol/the essential oil of Melaleuca alternifolia/water microemulsions. *Colloids and Surfaces A: Physicochemical and Engineering Aspects* **2009**, *348*, 289-297.

(42)   Sautina, N. V.; Galyametdinov, Y. G. Influence of propylene glycol on the formation of self-organizing structures in water / lecithine / vaseline oil systems. *Zhidkie Kristally i Ikh Prakticheskoe Ispol'zovanie* **2016**, *16*, 83-89.

(43)   Sautina, N.; Zakharova, A.; Galyametdinov, Y. Influence of Lecithin – Propylene Glycol Intermolecular Interactions at the Water / Vaseline Oil Interphase on the Formation of Self-Organizing Structures. *Liquid Crystals and their Application* **2017**, *17*, 35-41.

(44)   Lidich, N.; Wachtel, E. J.; Aserin, A.; Garti, N. Water-dilutable microemulsions for transepithelial ocular delivery of riboflavin phosphate. *Journal of Colloid and Interface Science* **2016**, *463*, 342-348.

(45)   El Maghraby, G. M. Transdermal delivery of hydrocortisone from eucalyptus oil microemulsion: Effects of cosurfactants. *International Journal of Pharmaceutics* **2008**, *355*, 285-292.

(46)   El Maghraby, G. M. Occlusive and non-occlusive application of microemulsion for transdermal delivery of progesterone: Mechanistic studies. *Scientia Pharmaceutica* **2012**, *80*, 765-778.

(47)   Martino, A.; Kaler, E. W. Phase behavior and microstructure of nonaqueous microemulsions. *Journal of Physical Chemistry* **1990**, *94*, 1627-1631.

(48)   Martino, A.; Kaler, E. W. Phase behavior and microstructure of nonaqueous microemulsions. *Langmuir* **1995**, *11*, 779-784.

(49)   Binks, B.; Kellay, H.; Meunier, J. Effects of Alkane Chain Length on the Bending Elasticity Constant K of AOT Monolayers at the Planar Oil-Water Interface. *EPL (Europhysics Letters)* **1991**, *16*, 53.

(50)   McKee, R. H.; Adenuga, M. D.; Carrillo, J.-C. Characterization of the toxicological hazards of hydrocarbon solvents. *Critical Reviews in Toxicology* **2015**, *45*, 273-365.

(51)   Godoy, C. A.; Valiente, M.; Pons, R.; Montalvo, G. Effect of fatty acids on self-assembly of soybean lecithin systems. *Colloids and Surfaces B: Biointerfaces* **2015**, *131*, 21-28.

(52)   Ontiveros, J. F.; Pierlot, C.; Catté, M.; Molinier, V.; Pizzino, A.; Salager, J.-L.; Aubry, J.-M. Classification of ester oils according to their Equivalent Alkane Carbon Number (EACN) and asymmetry of fish diagrams of C10E4/ester oil/water systems. *Journal of Colloid and Interface Science* **2013**, *403*, 67-76.

(53)   Hall, R. L.; Oser, B. L. Recent Progress in the Consideration of Flavoring Ingredients Under the Food Additives Amendment III. GRAS Substances. *Food Technology* **1965**, *19*, 151-197.

(54)   Schulman, J. H.; Stoeckenius, W.; Prince, L. M. Mechanism of Formation and Structure of Micro Emulsions by Electron Microscopy. *The Journal of Physical Chemistry* **1959**, *63*, 1677-1680.

(55)   Eastoe, J.; Sharpe, D. Properties of phosphocholine microemulsions and the film rigidity model. *Langmuir* **1997**, *13*, 3289-3294.

(56)   Bird, D. A.; Laposata, M.; Hamilton, J. A. Binding of ethyl oleate to low density lipoprotein, phospholipid vesicles, and albumin: A 13C NMR study. *Journal of Lipid Research* **1996**, *37*, 1449-1458.

(57)   Silber, J. J.; Biasutti, A.; Abuin, E.; Lissi, E. Interactions of small molecules with reverse micelles. *Advances in Colloid and Interface Science* **1999**, *82*, 189-252.

(58)   Balogh, J.; Olsson, U.; Pedersen, J. S. Dependence on Oil Chain Length of the Curvature Elastic Properties of Nonionic Surfactant Films: Emulsification Failure and Phase Equilibria. *Journal of Dispersion Science and Technology* **2006**, *27*, 497-510.

(59)	Deen, G. R.; Pedersen, J. S. Phase Behavior and Microstructure of C12E5 Nonionic Microemulsions with Chlorinated Oils. *Langmuir* **2008**, *24*, 3111-3117.

(60)	Hishida, M.; Yanagisawa, R.; Usuda, H.; Yamamura, Y.; Saito, K. Communication: Rigidification of a lipid bilayer by an incorporated n -alkane. *Journal of Chemical Physics* **2016**, *144*.

(61)	Abràmoff, M. D.; Magalhães, P. J.; Ram, S. J. Image processing with imageJ. *Biophotonics International* **2004**, *11*, 36-41.

(62)	Khattab, I. S.; Bandarkar, F.; Khoubnasabjafari, M.; Jouyban, A. Density, viscosity, surface tension, and molar volume of propylene glycol+water mixtures from 293 to 323K and correlations by the Jouyban–Acree model. *Arabian Journal of Chemistry* **2017**, *10*, S71-S75.

(63)	SasView application: http://www.sasview.org/.

(64)	Petelska, A. D.; Figaszewski, Z. A. The equilibria of phosphatidylcholine-fatty acid and phosphatidylcholine-amine in monolayers at the air/water interface. *Colloids and Surfaces B: Biointerfaces* **2011**, *82*, 340-344.

(65)	He, F.; Li, R. X.; Wu, D. C. Monolayers of mixture of alkylaminomethyl rutin and lecithin at the air/water interface. *Journal of Colloid and Interface Science* **2010**, *349*, 215-223.

(66)	Hac-Wydro, K.; Wydro, P. The influence of fatty acids on model cholesterol/phospholipid membranes. *Chemistry and Physics of Lipids* **2007**, *150*, 66-81.

(67)	Considine, D. M.: *Foods and Food Production Encyclopedia*; Springer US, 2012.

(68)	May, S.; Ben-Shaul, A. Spontaneous curvature and thermodynamic stability of mixed amphiphilic layers. *The Journal of Chemical Physics* **1995**, *103*, 3839-3848.

(69)	Chaieb, S.; Binks, B.; Meunier, J. Effects of Mixtures of Alkanes on the Bending Rigidity Constant K of AOT Monolayers at the Planar Oil-Water Interface. *http://dx.doi.org/10.1051/jp2:1995184* **1995**, *5*.

(70)	Helfrich, W. Elastic properties of lipid bilayers: theory and possible experiments. *Zeitschrift fur Naturforschung. Teil C: Biochemie, Biophysik, Biologie, Virologie* **1973**, *28*, 693-703.

(71)	Rawicz, W.; Olbrich, K. C.; McIntosh, T.; Needham, D.; Evans, E. Effect of chain length and unsaturation on elasticity of lipid bilayers. *Biophysical journal* **2000**, *79*, 328-339.

(72)	Ezrahi, S.; Tuval, E.; Aserin, A.; Garti, N. The effect of structural variation of alcohols on water solubilization in nonionic microemulsions: 1. From linear to branched amphiphiles - General considerations. *Journal of Colloid and Interface Science* **2005**, *291*, 263-272.

(73)	Ezrahi, S.; Tuval, E.; Aserin, A.; Garti, N. The effect of structural variation of alcohols on water solubilization in nonionic microemulsions: 2. Branched alcohols as solubilization modifiers: Results and interpretation. *Journal of Colloid and Interface Science* **2005**, *291*, 273-281.

(74)	Falcone, R. D.; Correa, N. M.; Silber, J. J. On the formation of new reverse micelles: A comparative study of benzene/surfactants/ionic liquids systems using uv-visible absorption spectroscopy and dynamic light scattering. *Langmuir* **2009**, *25*, 10426-10429.

(75)	Coster, H. G. L.; Laver, D. R. The effect of temperature on lipid-n-alkane interactions in lipid bilayers. *BBA - Biomembranes* **1986**, *857*, 95-104.

(76)	Bryant, G.; Taylor, M. B.; Darwish, T. A.; Krause-Heuer, A. M.; Kent, B.; Garvey, C. J. Effect of deuteration on the phase behaviour and structure of lamellar phases of phosphatidylcholines – Deuterated lipids as proxies for the physical properties of native bilayers. *Colloids and Surfaces B: Biointerfaces* **2019**, *177*, 196-203.

(77) Hughes, Z. E.; Malajczuk, C. J.; Mancera, R. L. The effects of cryosolvents on DOPC-β-sitosterol bilayers determined from molecular dynamics simulations. *Journal of Physical Chemistry B* **2013**, *117*, 3362-3375.

(78) Malajczuk, C. J.; Hughes, Z. E.; Mancera, R. L. Molecular dynamics simulations of the interactions of DMSO, mono- and polyhydroxylated cryosolvents with a hydrated phospholipid bilayer. *Biochimica et Biophysica Acta - Biomembranes* **2013**, *1828*, 2041-2055.

(79) Pilsl, H.; Hoffmann, H.; Hofmann, S.; Kalus, J.; Kencono, A. W.; Lindner, P.; Ulbricht, W. Shape investigation of mixed micelles by small angle neutron scattering. *Journal of Physical Chemistry* **1993**, *97*, 2745-2754.

(80) Bergström, M.; Pedersen, J. S. A Small-Angle Neutron Scattering (SANS) Study of Tablet-Shaped and Ribbonlike Micelles Formed from Mixtures of an Anionic and a Cationic Surfactant. *Journal of Physical Chemistry B* **1999**, *103*, 8502-8513.

(81) Goltsov, A. N.; Barsukov, L. I. Synergetics of the membrane self-assembly: A micelle-to-vesicle transition. *Journal of Biological Physics* **2000**, *26*, 27-41.

(82) Bergström, L. M. Bending Energetics of Tablet-Shaped Micelles: A Novel Approach to Rationalize Micellar Systems. *ChemPhysChem* **2007**, *8*, 462-472.

(83) Benedetto, A.; Heinrich, F.; Gonzalez, M. A.; Fragneto, G.; Watkins, E.; Ballone, P. Structure and stability of phospholipid bilayers hydrated by a room-temperature ionic liquid/water solution: A neutron reflectometry study. *Journal of Physical Chemistry B* **2014**, *118*, 12192-12206.

(84) Heberle, F. A.; Marquardt, D.; Doktorova, M.; Geier, B.; Standaert, R. F.; Heftberger, P.; Kollmitzer, B.; Nickels, J. D.; Dick, R. A.; Feigenson, G. W.; Katsaras, J.; London, E.; Pabst, G. Subnanometer Structure of an Asymmetric Model Membrane: Interleaflet Coupling Influences Domain Properties. *Langmuir* **2016**, *32*, 5195-5200.

(85) Bergström, L. M. Bending elasticity of charged surfactant layers: The effect of mixing. *Langmuir* **2006**, *22*, 6796-6813.

(86) Serafin, A.; Figaszewski, Z. A.; Petelska, A. D. Phosphatidylcholine-fatty Alcohols Equilibria in Monolayers at the Air/Water Interface. *Journal of Membrane Biology* **2015**, *248*, 767-773.

(87) Langmuir, I. The constitution and fundamental properties of solids and liquids. II. Liquids. *Journal of the American Chemical Society* **1917**, *39*, 1848-1906.